N 68 33446

NASA CR 96293

Semiannual Phase Report No. 1

LEAD TELLURIDE BONDING AND SEGMENTATION STUDY

Covering period

August 1, 1967 - January 31, 1968

Contract No. NAS 5-9149

Prepared by

Tyco Laboratories, Inc.

Bear Hill

Waltham, Massachusetts 02154

for

National Aeronautics and Space Administration

Goddard Space Flight Center

Greenbelt, Maryland 20771

Tyco Laboratories, Inc.
Bear Hill
Waltham, Massachusetts 02154

Lead Telluride Bonding and Segmentation Study

Semiannual Phase Report No. 1

Covering period
August 1, 1967 - January 31, 1968

Contract No. NAS 5-9149

by

H. Bates
F. Wald
M. Weinstein

for

National Aeronautics and Space Administration
Goddard Space Flight Center
Greenbelt, Maryland 20771

SUMMARY

I. Constitutional Studies

A. Tin-Telluride-Metal-Systems

Accurate lattice constant determinations on SnTe as incorporated in SnTe-Metal alloys revealed changes in the original lattice constant of the starting $Sn_{.492}Te_{.508}$ composition.

From these findings it has to be concluded that PbTe-SnTe thermoelectric alloys in contact with metals might change their composition and therefore their electrical properties over long periods of time.

Since such conditions could be important for the mechanism of aging of tungsten contacts to 3P material, a more thorough investigation of similar changes in the W-PbTe-SnTe system is indicated.

B. Silicon-Germanium-Metal-Alloys

Investigations of the interaction of Si-Ge solid solution alloys with Ti, Zr, V, Nb, Ta, Cr, Mo, W, Mn, Re and Co have revealed two basic types of constitution. The first is one in which equilibria between Si-Ge solid solutions and solid solutions of metal silicides and germanides exist. The elements Ti, Zr, Ta, and Co apparently belong to this category. The second type of system produces a metal silicide in equilibrium with either pure Ge or with the Si-Ge solid solution. Elements behaving in this fashion are W, V, Nb, Cr, Mo, Mn, and Re. It was also found that phosphorous present as a dopant in n-type Si-Ge was concentrated in the $MoSi_2$ formed by addition of Mo. This is taken to indicate that metal phosphides (and presumably borides in the p-type material) can form and apparently dissolve in the metal silicide.

II. Segmented Si-Ge-PbTe Thermocouples

Measurements of the efficiency of segmented couples have shown efficiencies of approximately 9% at hot junction temperatures of 800° and above, and power outputs of 2.25 to 2.8 watts per couple.

III. Pore Migration

Quantitative metallography has shown evidence for fairly extensive migration of pores in pressed-and-sintered $Pb_{.4}Sn_{.6}Te$ thermoelements after operation for 3800 hours in a temperature gradient from 510° to 50°C.

IV. Life Testing

A. Isothermal Testing

Tungsten bonds to 3P elements have been tested to 6000 hours at 525°C. One half of the bonds remained intact; those measured showed an increase to 95 $\mu\Omega$ - cm^2 contact resistivity from an initial value of 16 $\mu\Omega$ - cm^2.

B. Gradient-Testing of W-Bonded 3N-3P Couples

Six of fourteen bonded couples tested to 800 hours at a hot junction temperature of approximately 520°C survived approximately 35 unscheduled thermal cycles with unchanged total resistance.

C. Gradient-Testing of W-Bonded 3P Elements

Post-test analysis of gradient tested elements showed decreased resistivity and Seebeck voltage at hot ends of elements and precipitation of extensive amounts of an unidentified phase at intermediate and high temperatures.

CONTENTS

CONTENTS (cont.)

LIST OF ILLUSTRATIONS

LIST OF ILLUSTRATIONS (cont.)

LIST OF TABLES

I. INTRODUCTION

The widespread use of thermoelectric power generation has been anticipated for some years as the solution to a number of specialized power-supply problems. However, the application of thermoelectrics has been hindered by a number of major materials problems. These problems can be divided into those associated with (1) the physical characteristics, (2) the chemical behavior, and (3) the low conversion efficiency of thermoelectric materials.

The predominantly covalent nature of most thermoelectric alloys results in materials which are generally weak and brittle. In addition, PbTe alloys have a high thermal expansion coefficient which leads to susceptibility to thermal shock and thermal stress cracking. The mismatch in expansion coefficient between PbTe and metals also causes a fundamental physical incompatability which must be dealt with in contacting these materials at the hot side. The vapor pressure of PbTe alloys precludes operation in vacuum or requires encapsulation. Porosity in sintered PbTe not only contributes to their mechanical instability, but may also pose a substantial long-term hazard to the integrity of metallurigical bonds by migration of the pores in the temperature gradient. The high temperature mechanical properties of PbTe alloys are very poorly defined, and there is almost a complete lack of understanding as to what role they may have in generator design.

The reactive nature of one or more elements in all thermoelectric materials places severe limitations on the materials for use as hot side contacts. Reaction between the metal contact and the thermoelectric material can produce electrically active or mechanically destructive phases at the interface. Interactions between the dopants and contacts are also possible which can drastically affect the electrical properties. In fact, the consequences of reaction between the thermoelectric material and any of the several materials which constitute its environment are such that extreme care must be exercised in the choice of all such materials. However, without a basic knowledge of the interactions of the thermoelectric

material with metals, potential brazes, insulations, and so forth, selection of these materials can only be by a trial and error process.

The low efficiency of thermoelectric generating materials has been the main impediment to their wider application as power sources. The search for new materials has been largely abandoned. However, the need for higher efficiencies still exists. The most feasible means for achieving higher efficiencies appears to be the combination of existing materials over extended temperature ranges. The best known thermoelectric power generation materials, PbTe and Si-Ge, have optimum temperature ranges which complement each other for operation over a temperature interval of 800 - 1000°C to 200 - 50°C. Devices utilizing these materials over such a temperature interval should exhibit higher conversion efficiency than either material alone.

This program comprises a study of (1) the bonding of PbTe thermoelements to nonmagnetic electrodes, (2) the behavior of the elements and contacts at operational temperatures, (3) the compatibility of PbTe and SnTe with metals and the interactions of Si-Ge thermoelectric materials with potential hot contact materials and brazes, and (4) the physical and chemical characteristics of the PbTe thermoelements. Other aspects of the program include a study of the segmenting of Si-Ge thermoelements with PbTe for higher efficiency, life testing of PbTe thermoelements and couples, design and construction of a prototype test device for Si-Ge-PbTe thermocouples, and the design of modules incorporating W-bonded PbTe and segmented SiGe-PbTe.

The general aim of the program is to define the most appropriate system and process for the preparation of low-resistance, high strength bonds of nonmagnetic electrodes to PbTe alloys and to study the factors and processes involved in the degradation of thermoelements and contacts during extended service.

II. CONSTITUTIONAL STUDIES

A. Systems Containing Tin Telluride

1. Introduction

In past work under this contract, chemical reactions of lead telluride and tin telluride with metals have been discussed at length and, to a large extent experimentally verified.

The conclusions were based on determining the direction of the reaction

$$ATe + M \quad \rightarrow \quad MTe + A \tag{1}$$

where A is lead or tin and M is a metal. This reaction constitutes a major degradation mode in thermoelectric junctions if it operates in the indicated direction, has a finite speed in the period of use of the device, and produces electrically active or mechanically destructive phases. Nevertheless, it must be recognized that (1) is not the only possibility of producing second phases in the vicinity of a junction between a metal and a thermoelectric material. This is particularly true if the thermoelectric material is constituted of a complex mixture.

It is, however, also immediately clear that for every heterogeneous constituent in a mixture a reaction equation similar to (1) can be written separately in order to describe the over-all reaction behavior.

Thus, for a material which might be constituted (as an arbitrary example) of a heterogeneous mixture of a lead-tin-telluride solid solution, manganese telluride and excess tellurium, one could obviously write

$$(Pb_x Sn_y) \, Te + M \quad \rightleftharpoons \quad MTe + xPb + ySn \tag{2a}$$

$$MnTe + M \quad \rightleftharpoons \quad MTe + Mn \tag{2b}$$

$$Te + M \rightleftharpoons M \, Te \tag{2c}$$
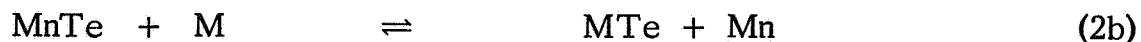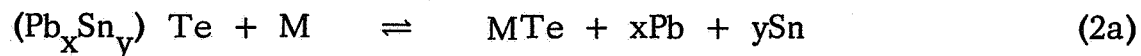
(M = metal)

Reaction 2(c), due to the reactivity of Te is virtually certain to proceed from left to right.

As a second step, it would be necessary to evaluate the possibility of secondary reactions between the reaction products of eqs. (2a-c). All this, even if it seems rather cumbersome to do so in practice, can be evaluated by thermodynamic means.

But there are yet more subtle forms of interaction which might lead to undesirable electrical results in the junctions or in the material. These are separate reactions of the homogeneous constituents of the materials.

If one evaluates eq. (2a), such a case can be envisioned if we assume that the lead in the solid solution will react differently from the tin, which in contact with certain metals is a quite feasible proposition. More subtle yet and indeed quite dangerous are the reactions which a dopant might undergo to form an insoluble complex with a contacting material, depleting the carrier concentration in the thermoelectric material.

In the case of tin telluride and lead telluride-tin telluride solid solutions, an especially interesting example of this occurs.

To understand the facts correctly, it is necessary to discuss in somewhat more detail the special properties of SnTe which are pertinent to the behavior of PbTe-SnTe solid solutions.

Tin telluride possesses, as does lead telluride, the sodium chloride structure. Materials crystallizing in this structure usually possess cation to anion ratios close to 1:1. In lead telluride certain deviations are found, but these are quite small (in the order of 0.01%).

Tin telluride, however, being on the verge of a structural change (SnSe and GeTe possess different structures)shows strong deviations from a 1:1 SnTe ratio. The single-phase range of the compound does, in fact, never reach the 1:1 ratio, 50.1 at % Te being the lowest Te content possible[1, 2]. Also, the Te content can reach as high as 51.1% as shown by Brebrick[1] and Umeda, et al.[2]. These authors demonstrate furthermore that the tin

- 4 -

vacancies, to be assumed in the structure, strongly influence the carrier concentration. Firstly, they keep SnTe p-type under all conditions. Secondly, the p-type carrier concentration can be changed from 3.88 . 10^{20}/cm^3 at 50.1 at % Te to 18.4 . 10^{20}/cm for material Te saturated at 550°C[1]. The latter material contains ~ 51.1 at % Te. SnTe is therefore a quite effective p-type dopant, the carrier concentration depending on the excess of tellurium (creation of Sn-vacancies!) in the structure.

Use of these properties of tin telluride as a dopant can be made in lead telluride-tin telluride solid solutions only if the homogeneous phase range extends across the pseudobinary section SnTe-PbTe. That this is so becomes apparent from the use of these alloys as p-type thermoelectric materials. Only recently[3, 4] has this been experimentally proven however, and the details of the phase field are still being investigated.

In our previous investigations on the reactions of SnTe, the excess of tellurium found in homogeneous solid solution has not been taken into account. Most alloys were made with SnTe of 50.8 at % Te content. This, according to previous investigations[1, 2], constitutes the maximum melting and thus most stable (lowest free energy) composition in the system.

In the following it is demonstrated that in the presence of metals or metal-rich tellurides, the most stable SnTe in the equilibrium is one of much lower Te content. Conclusions from this which are pertinent to thermoelectrics are then discussed.

2. Experimental Results

Brebrick[1] has presented the change in lattice parameter of SnTe from the tin rich side to the tellurium rich side at various temperatures. He also notes that the phase lattitude is largest at 600°C. Table I gives his lattice parameter results, together with our own. Our values were gained from exposing material in a 114.6 diameter Norelco camera with nickel filtered copper radiation for 8 hours. The measured distances of the lines

TABLE I

Lattice Parameters of Various Compositions of Tin Telluride

Material Spec.	Composition of Single Phase Limit	Temp. °C	Investigator	Lattice Parameter Å
Sn-saturated SnTe	~ 50.3 at % Te	772	Brebrick[1]	6.318±0.002
SnTe-as grown		---	"	6.314±0.001
Te saturated SnTe	~ 50.7 at % Te	706	"	6.308±0.001
Te saturated SnTe	~ 51.0 at % Te	550	"	6.306±0.001
SnTe as cast	50.8 at % Te	---	Tyco	6.308±0.003
$Sn_{.5}Te_{.5}$ annealed	~ 50.1 at % Te	600	Tyco	6.327±0.004
$Sn_{.48}Te_{.52}$ annealed	~ 51.1 at % Te	600	Tyco	6.300±0.002

on the film were corrected for film shrinkage and were converted to d-spacings using an available computer program.

The diffraction spectra obtained were indexed with the help of the ASTM file. After indexing, the d-spacings were fed into a computer and extrapolated against the Nelson-Riley function[5] to a 90° θ angle by a least squares method. The computer method also calculates a standard deviation of all d-spacings from the least squares line. This standard deviation is taken as our error. It can be seen that quite reasonable agreement with the reported values is achieved.

Examining the lattice parameter values of SnTe in hetero-geneous mixtures of SnTe and metal, using alloys described before[6-8], should allow conclusions as to whether the SnTe used (with 50.8 at % Te) lost any Te when equilibrated with a metal. If Te is lost, the lattice constant should shift from the value of 6.308 Å found for a 50.8 at % Te composition to higher values, indicating less Sn vacancies.

Table II shows the results for all SnTe metal mixtures in-vestigated. The alloys are situated in various phase fields, which are not futher discussed but can be obtained from (6-8). Common to all alloys is, however, that they contain SnTe and a metal or metal-rich compound.

It can be seen that in all cases investigated, with the sole exception of copper, the lattice parameter increased from the value of 6.308 Å of the starting material. This indicates filling-up of tin vacancies for all cases.

In principle, this might not only be due to a loss of Te but also to the metal entering vacant tin sites. Ancillary evidence, such as the appearance of small amounts of a third phase in many of the alloys where it was not expected (Au, Mo, etc.), indicates loss of tellurium and subsequent formation of metal-telluride. The electrical effects, however, are equally severe for the first possibility since, no matter how, loss of Sn vacancies means loss of p-type carriers.

TABLE II

Lattice Parameters of Tin Telluride in Alloys
With Metals

Composition as Stoichiometries	Lattice Parameter $\overset{\circ}{A}$
2 SnTe + Mo	6.314 ± 0.006
SnTe + 3 Fe	6.319 ± 0.001
SnTe + Co	6.323 ± 0.004
SnTe + Ni	6.317 ± 0.007
SnTe + NiTe	6.318 ± 0.004
SnTe + Ni$_{.6}$Sn$_{.4}$	6.320 ± 0.004
SnTe + 2 Cu	6.304 ± 0.008
SnTe + 2 Ag	6.315 ± 0.006
2 SnTe + Ag$_2$Te	6.316 ± 0.004
SnTe + Ag$_2$Te	6.314 ± 0.004
SnTe + 2 Ag$_2$Te	6.312 ± 0.006
2 SnTe + Au	6.314 ± 0.003

In the case of copper where an exception is observed, a solid solution of SnTe-CuTe may be formed which would make conclusions more difficult.

3. Discussion and Conclusions

The results of the X-ray analyses presented make it quite clear that SnTe in equilibrium with a metal or a metal rich compound does indeed have a different and usually rather low Sn-vacancy content. It may be expected and presumably could be proven by lattice parameter measurements that in PbTe-SnTe solid solutions this is also the case.

Thermoelectric materials therefore will be affected electrically if one relies on the doping by Sn vacancies in excess of the equilibrium concentration tolerated by the total PbTe-SnTe-Admixture-Contact Material system. It is suspected that the appearance of small amounts of tellurides in some systems may be due to this cause and electrical changes are to be expected then.

Furthermore, in such a case the definition of "free tellurium" being present in a material will have to be expanded to not only include the truly free. elemental, second phase tellurium, but also tellurium which may be originally dissolved but is "free" to react with a metal until an equilibrium is achieved. The investigations cited will be carried out in detail for various lead telluride-tin telluride tungsten alloys, annealed at 450, 500, 550, 600 and 830°C to study this aspect of reaction in relation to the tungsten diffusion bond.

B. Systems Containing Silicon-Germanium

1. Introduction

For the high temperature operation of junctions to Si-Ge thermocouples, it seems desirable to possess some knowledge of phase equilibria. Such knowledge is equally desirable whether metal bridges or silicide bridges and solders are used. To predict long-term degradation modes in such junctions, it is always helpful

to be informed about the final thermodynamic state which the system ultimately would want to achieve. If dopants (B or P) or admixtures to the brazes (e.g. C)[9] are also present, the modification of Si-Ge metal equilibria by these elements should also be considered.

In general, information on ternary phase equilibria containing Si-Ge and metals is scarce.

W-Si-Ge has been investigated by Nowotny and his group[10], along with V-Si-Ge[11] and Th-Si-Ge[12]. These systems show some prototypes of equilibria to be expected in the solid state. Unfortunately, temperatures of solid-liquid equilibria (eutectics, etc.) have not been studied in any of these systems although in some of them where free Ge appears, there may be eutectics at rather low temperatures (e.i. below the melting point of Ge).

Brixner has reported on some pseudobinary solid solution systems such as $U Si_3$-$U Ge_3$[13], $Ta Si_2$-$Ta Ge_2$ and $NbSi_2$-$NbGe_2$[14]. All these latter systems were found to form continuous solid solution series. It was also found that these solid solutions generally are of a metallic conduction type (i.e. low electrical resistivity, low Seebeck coefficient, high thermal conductivity). This latter behavior is quite desirable for the purposes discussed here.

Our own investigations have taken two different approaches. Firstly, a survey was conducted where special materials which contained 2 at % of various metals were procured from a commercial supplier of semiconductor type Ge-Si solid solutions.

The first batch of these contained 2 at % each of Ti, Zr, V, Nb, Ta, Cr, Mo, W, Mn, Re and Co in undoped Si-Ge. A second batch consisted of 1 at % Ti in both B-doped p-type material and P-doped n-type material and 1 at % Mo in both B-doped p-type materials and P-doped N-type materials. All metals were incorporated in the thermoelectric material during the original manufacturing process.

These materials were to be analyzed microscopically and by electronmicroprobe analysis.

The second approach is centered around the detailed investigation of three ternary systems: Co-Ge-Si, Ti-Ge-Si and Mo-Ge-Si. The interactions of boron and phosphorous in these systems will also be studied.

These systems have been selected for reasons of (1) varying melting points in the constituent binaries, and (2) possible (and for Mo-Si-Ge already practical) application as bridge materials and/or brazes.

2. Experiments and Results

a. Electron Microprobe Analysis*

(1) Studies on undoped Si-Ge solid solutions with 2 at % metal addition.

These studies may best be summarized by placing all elements into two general groups. Elements in the first group show solid solutions of Si-Ge to be in equilibrium with solid solutions between silicides and germanides.

These elements are Ti, Zr, Ta and Co. (The latter is questionable because of the small size of the particles.) The second group of elements contains those where silicides with no or very small Ge additions are found. It is thus to be assumed that here the silicide only is in equilibrium with the Si-Ge solid solution or with pure Ge. The silicide may dissolve a small amount of Ge, however. Prototypes for this kind of system are W-Si-Ge[2] and V-Si-Ge[3]. Elements found to behave in the latter way are the two prototypes W and V, as well as Nb, Cr, Mo, Mn, Re.

---

* The authors are indebted to Mr. Larry Kobren of Goddard Space Flight Center NASA, who carried out all of the electronmicroprobe analysis work.

Quantitative analysis (error $\sim \pm 10\%$ relative by weight for each element) indicates that in the Ti-Si-Ge system the solid solution is between $TiSi_2$ and $TiGe_2$ with $\sim 10\%$ $TiGe_2$ present in the alloy investigated here.

Primary crystals in the Cr-Si-Ge system are indicated to be $CrSi_2$ and in the Mn-Si-Ge system MnSi is found.

In all cases investigated it was found that the formerly homogenous Si-Ge solid solution was badly segregated after metal introduction so that it is not possible to make any estimations on the equilibrium concentrations.

(2) Studies on doped Mo-Si-Ge (B+P) and Ti-Si-Ge (B and P) alloys.

In both cases analysis of boron was impossible because of the limitations of the microprobe.

In both phosphorous doped systems an increase in phosphorous content in the metal silicide or metal silicogermanide was found. In the case of Mo-Si-Ge it was determined that the phosphorous content in the $MoSi_2$ crystals was 5 times as high as in the matrix. It must therefore be concluded that in both cases investigated (Mo and Ti) a tendency for the formation of phosphides exists. The phosphides formed apparently go into solid solution with the silicides.

b. Phase Equilibrium Studies

The electron microprobe analyses showed clearly that the detailed study of the three prototypes Ti-Si-Ge, Mo-Si-Ge and Co-Si-Ge constitutes a representative choice of different prototype systems with broad practical implications. Studies on these systems have only just started and a number of experimental difficulties have become apparent. These difficulties are related to two major properties of the alloys to be investigated: (a) high reactivity and (b) slow establishment of equilibrium. The properties described under (a) result in difficulties of finding suitable crucible materials for thermal analysis, particularly for the higher melting systems containing Ti and Mo. The second group of properties requires long annealing times to achieve true equilibrium.

Only tentative results are therefore available on the systems so far. In Co-Si-Ge it becomes clear that most probably a pseudobinary section CoSi-Ge exists in the system. This section has a low melting eutectic at ~ 815°C.

There does not seem to exist a pseudobinary section between $CoSi_2$ and Ge. Alloys on this section show three phase equilibria consisting of $CoSi_2$-CoSi and (Si-Ge) with approximately 20% Si content. It is doubtful, however, whether the latter description represents equilibrium conditions.

At the present time detailed X-ray investigations on alloys which had been annealed for 1090 hrs at 760°C are underway. These should at least settle questions as to the CoSi-Ge and $CoSi_2$-Ge-Si equilibria. In the Ti-Si-Ge system the cast alloys were too confusing to allow any judgments and the problems of finding suitable crucibles for thermal analysis are also particularly severe in this system.

A number of alloys are being annealed but not even tentative conclusions can be reached in the system at the present time.

c. Conclusions

Some preliminary conclusions with regard to thermoelectric bonding may be reached from the work presented so far. From the microprobe analysis it becomes apparent that in certain systems solid solutions between silicides and germanides play a substantial role in the phase equilibria. No equilibria between compounds and the constituent elements of the Si-Ge solid solution seem to be present.

Such conditions are expected to favor high melting points. In these systems it is not expected that low melting eutectics will occur which might interfere with the operation of thermoelements up to perhaps 1000°C. However, pure silicide bridges of materials belonging to these alloy systems should be expected to degrade in the long run by dissolving some Ge from the thermoelement. To what extent this happens depends on the detailed phase equilibria. We hope to show a prototype of such an interaction in the Ti-Si-Ge system.

As a corollary to the above, silicides with low or no solubilities for germanium are to be favored as bridge materials.

The most significant finding so far is the proven diffusion of phosphorous dopant into molybdenum silicide. This will constitute a definite degradation factor in Mo-Si contacted Si-Ge thermoelements. Since we believe that phosphide formation and not solid solution of elemental phosphorous is responsible here, doping of the bridge with phosphorous will only slow down, but not halt, the process.

It is expected that much the same process happens in the case of boron although, because of the limitations of the microprobe, this cannot be proven.

The type of reactive diffusion envisioned here is expected to be very slow, but if lifetimes of a number of years are considered this degradation mode will have to be taken into account.

C. Investigations on the Tungsten Diffusion Bond Using Scanning Electron Microscopy

Scanning electron microscopy is a relatively new method which allows considerable magnification and high resolution of an opaque surface.[15]

This method was used on several tungsten diffusion bonded specimens.* It was hoped that high magnification might reveal some layers of a bonding substance in the interfaces between tungsten and lead telluride. Figures 1 - 4 show the scanning microscope photographs obtained from corresponding areas of a p-type tungsten diffusion bonded specimen at magnifications of 720 X, 2900 X, 6200 X and 14, 500 X, respectively.

No definitive indications of an interface layer could be found. It therefore has to be concluded that if such a layer is present (as it must be assumed to be), it is either extremely thin or does not provide any significant contrast in the electron beam in comparison to tungsten and/or lead telluride.

---

* The authors are indebted to Mr. R. F. Anstead of Goddard Space Flight Center, NASA, for providing the scanning electron microscope photographs and for helping in their interpretation.
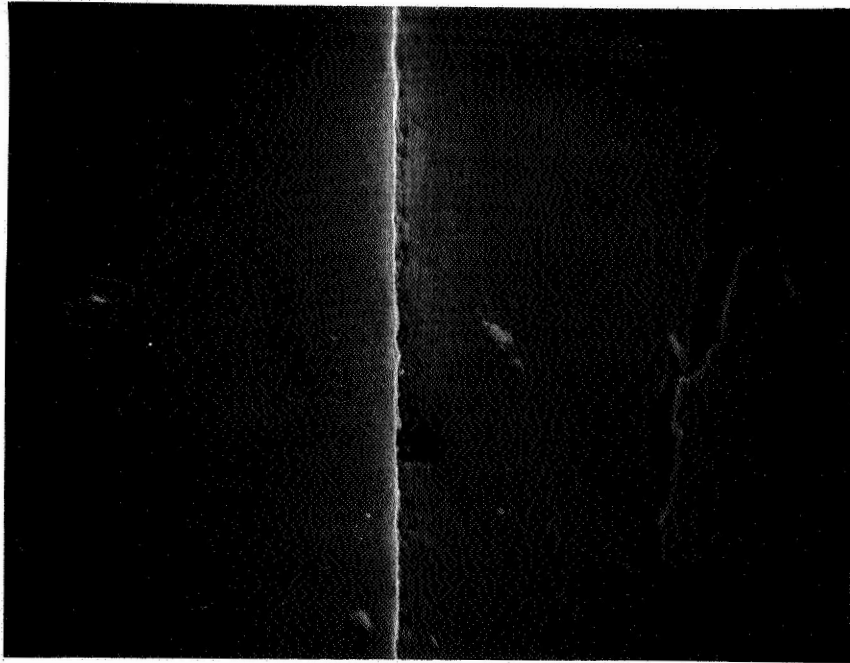
W   PbTe

Fig. 1   Scanning Electron micrograph of p-type (3P) tungsten
          diffusion bonded specimen.   Magnification: 720X
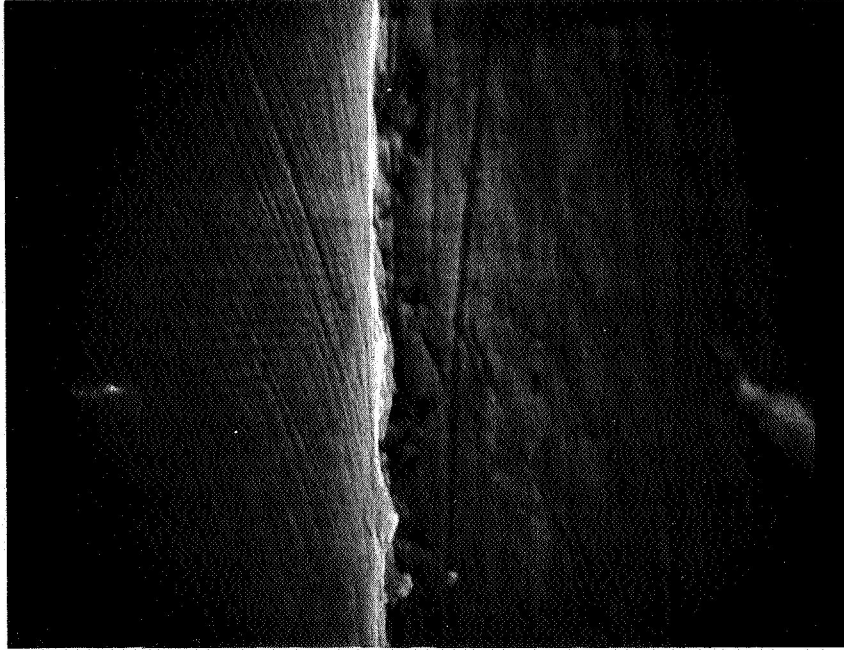
W   PbTe

Fig. 2   Scanning electron micrograph of p-type (3P) tungsten
          diffusion bonded specimen.   Magnification: 2900 X
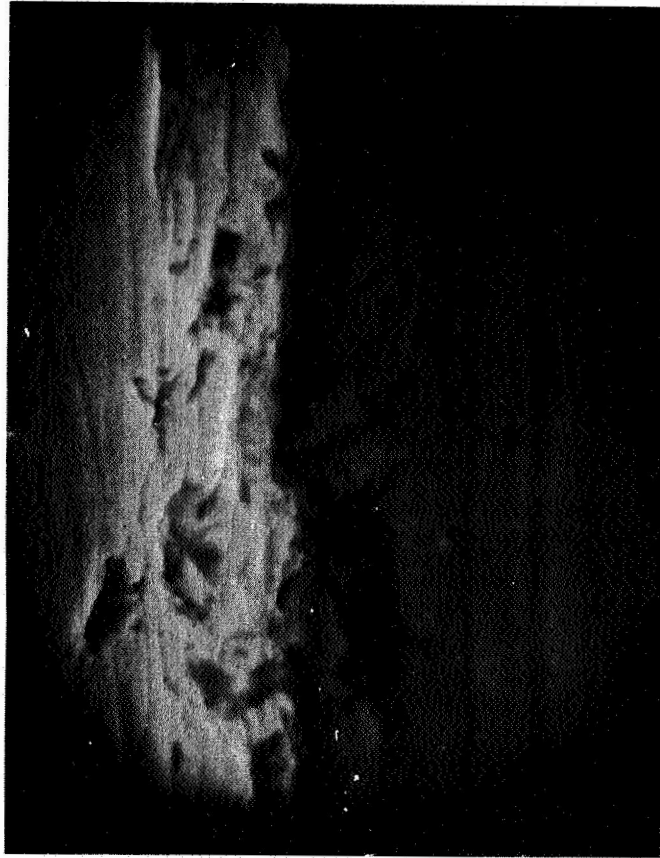
W   PbTe

Fig. 3 Scanning Electron Micrograph of p-type (3P)
tungsten diffusion bonded specimen. Magnification: 6200 X
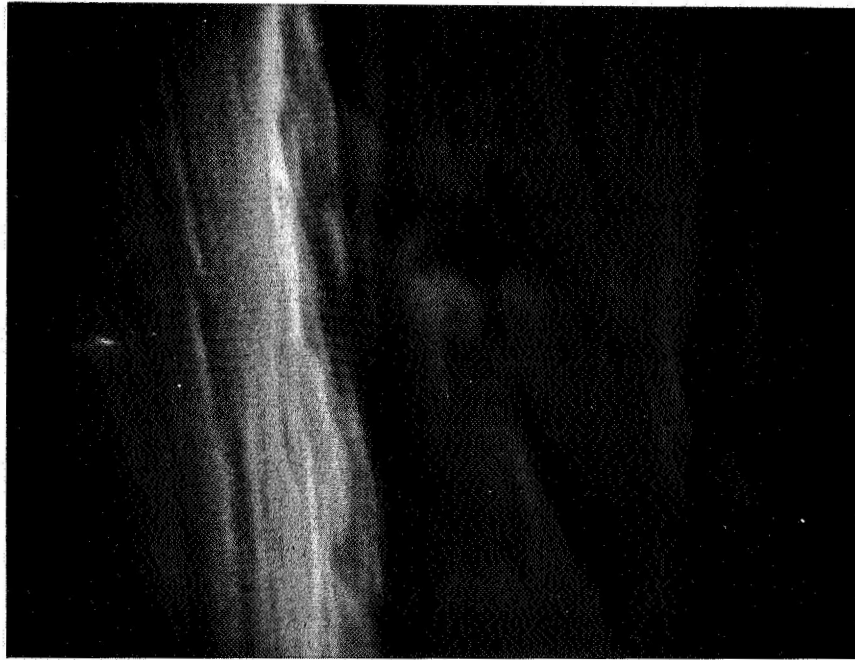
W   PbTe

Fig. 4 Scanning electron micrograph of p-type (3P) tungsten
        diffusion bonded specimen.   Magnification: 14, 500 X

III. SEGMENTED Si-Ge-PbTe THERMOCOUPLES

A. Introduction

The design and preparation of a segmented SiGe-PbTe couple for experimental measurements up to a hot junction temperature of 800°C was discussed in the Second Interim Summary Report. The couple was designed for maximum efficiency by treating the heat flow at the segment boundaries at zero current, then using the calculated shape ratios to calculate average values of ρ and K for the two legs. The theoretical efficiency can then be calculated as if the legs were single materials, using the equations

$$Z^* = \frac{(\bar{\alpha}_p + \bar{\alpha}_n)^2}{[(\bar{\rho}_p \cdot \bar{K}_p)^{\frac{1}{2}} + (\bar{\rho}_n \cdot \bar{K}_n)^{\frac{1}{2}}]^2} \tag{3}$$

$$M = (1 + Z^* T_{av})^{\frac{1}{2}} \tag{4}$$

$$\eta = \frac{T_H - T_C}{T_H} \frac{M - 1}{M + \dfrac{T_C}{T_H}} \tag{5}$$

The latter approach was used to design a segmented Si-Ge-PbTe couple for testing. Average properties for the segments were determined exactly by by graphical integration of the curves of properties vs. temperature. A drawing of the couple is shown in Fig. 5.

Calculations predict a maximum theoretical efficiency for this couple, operating between 800° and 50° with a 500°C intermediate temperature, of 9.85%. The actual operating efficiency is calculated to be 9.05%. The maximum power output is calculated to be 2.63 watts, delivered to a load of 10.4 m Ω. These predictions of performance include in the calculations the contact resistances which are expected to occur in an actual couple. The results of measurements on couples of this type are reported in the following section.
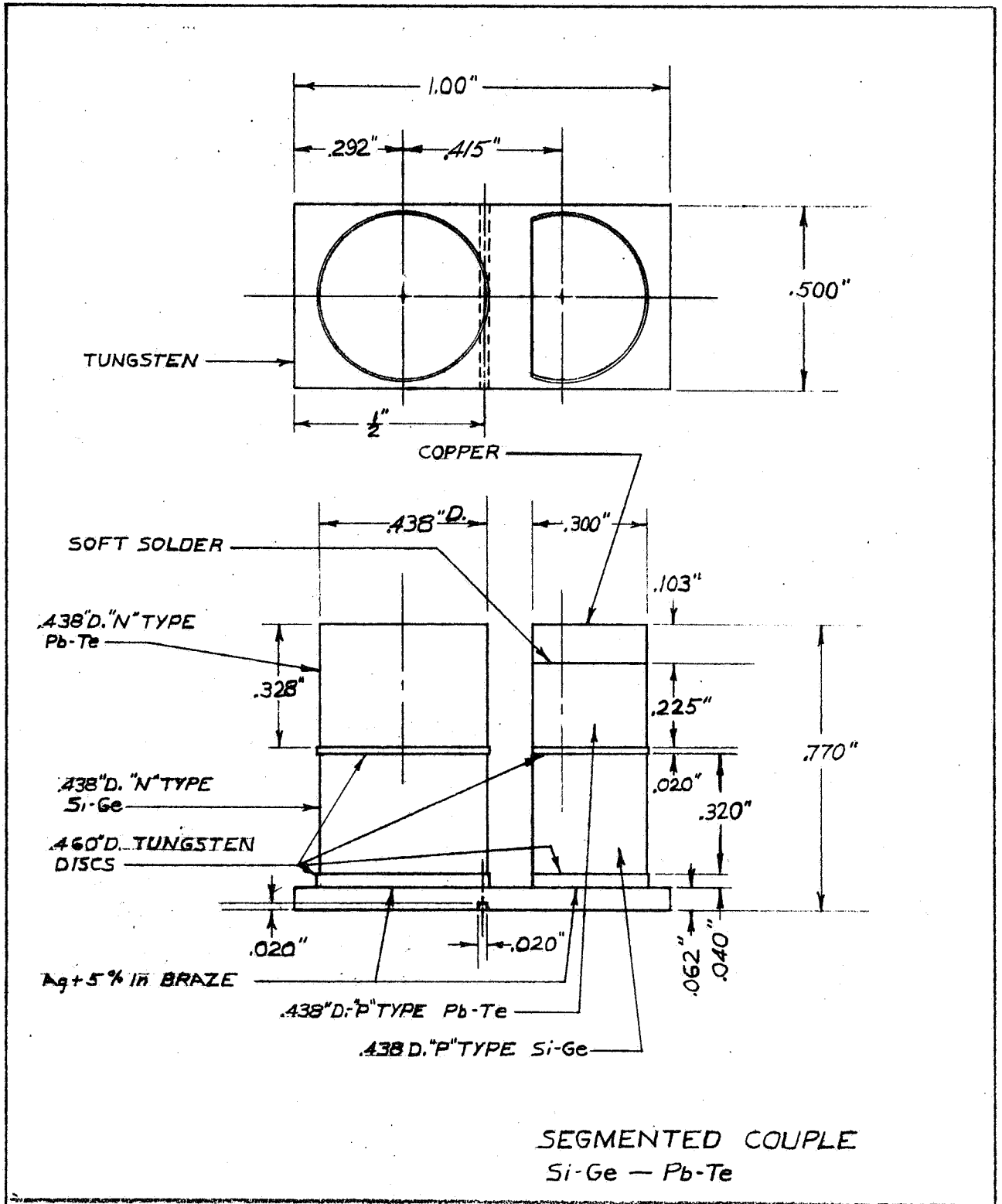
Fig. 5   Plan view and cross section of Si-Ge-PbTe couple for
testing and efficiency measurements.

Figure 6 shows the variation of theoretical efficiency with
temperature of PbTe, Si-Ge, and segmented Si-Ge-PbTe. The
efficiency for the single (paired) materials was calculated using
equations (3) - (5). The efficiency for the segmented materials
was calculated from the expression of equation (6) in conjunction

$$ Z^* = \frac{(\Sigma \bar{\alpha}_i)^2}{(\Sigma (\bar{\rho}_i \cdot \bar{K}_i)^{\frac{1}{2}})^2} \tag{6} $$

with (3) and (4). This gives results somewhat higher than those
obtained in the procedure used to design the segmented couples;
at 800°C the calculated efficiency is approximately 10.55%.
Applying this procedure to segmented Si-Ge-PbTe at a hot junction
temperature of 1000°C and cold junctions of 50° and 200°C gives
excellent agreement with the results of Rocklin[16] who recently
calculated the efficiency of segmented and cascaded Si-Ge-PbTe
between 1000°C and a range of cold junction temperatures.

Our calculations at hot junction temperatures of 1000°
and 800°C with a 200° cold junction for PbTe predict a theoretical
efficiency of 11.20% and 8.50% respectively for segmented Si-Ge-PbTe.

B. Measurements

The conversion efficiency is determined by measuring the
heat flux from the cold sides of the couple legs and the electrical
power output to a resistive load. The measurement apparatus was
described in detail previously. The technique presently used for
measurement of the heat flux required the addition of two copper
blocks under the thermocouple legs. The electrical circuitry is
unchanged. The apparatus is shown schematically in Fig. 7.

Heat is supplied to the hot strap of the couple by a resistance
heater at one end of the Ni block. The heat flowing from the cold
ends of the two legs is measured by measuring the temperature
difference between two thermocouples embedded at the centerline
of OFHC copper blocks. The spacing between the thermocouples

Fig. 6 Theoretical efficiency of PbTe, Si-Ge, and segmented
Si-Ge-PbTe.

HEATER

Ni - BLOCK

Si – Ge – PbTe COUPLE

INSULATION

COPPER BLOCKS
WITH THERMOCOUPLES

WATER COOLED
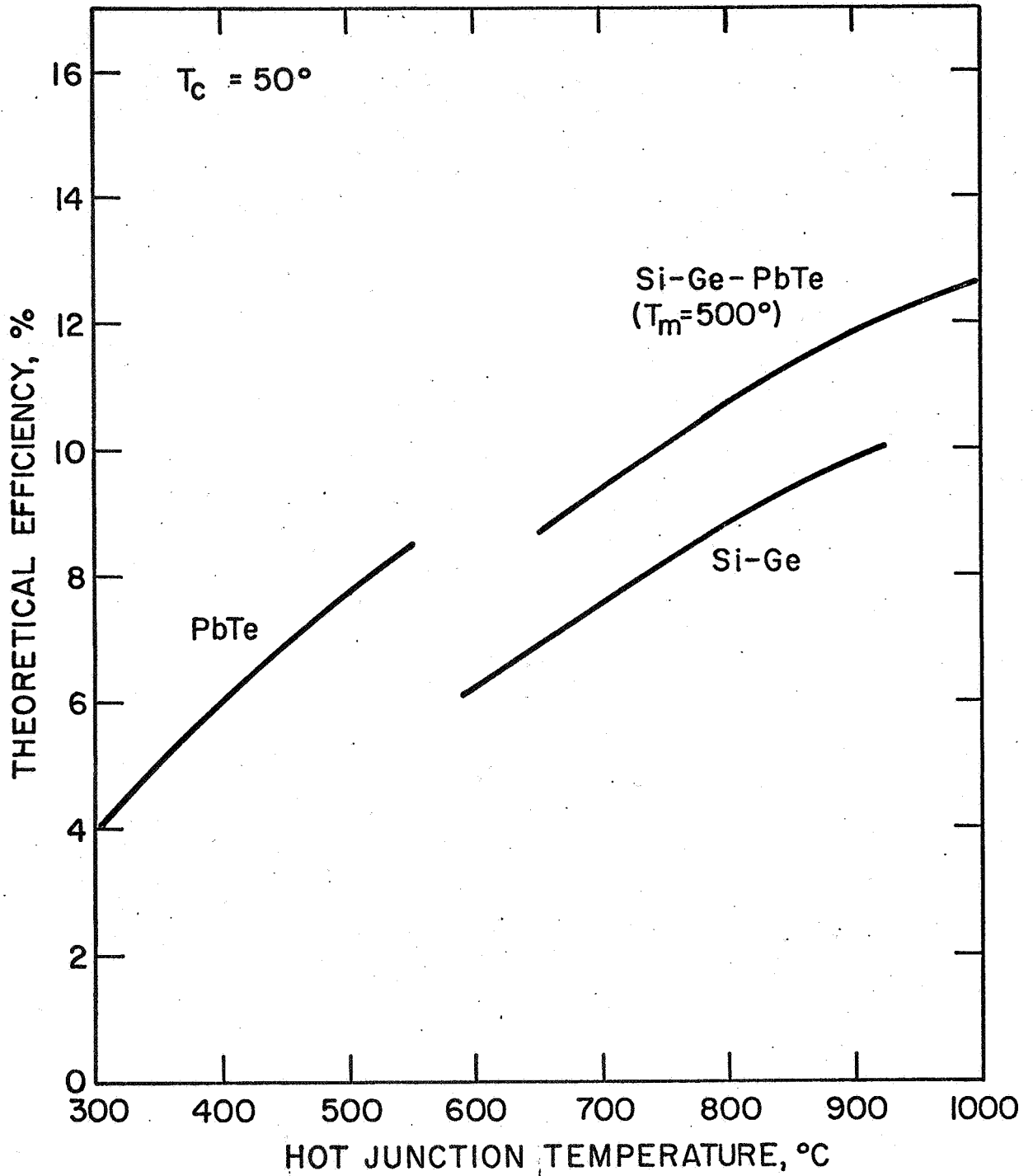COPPER PEDESTALS
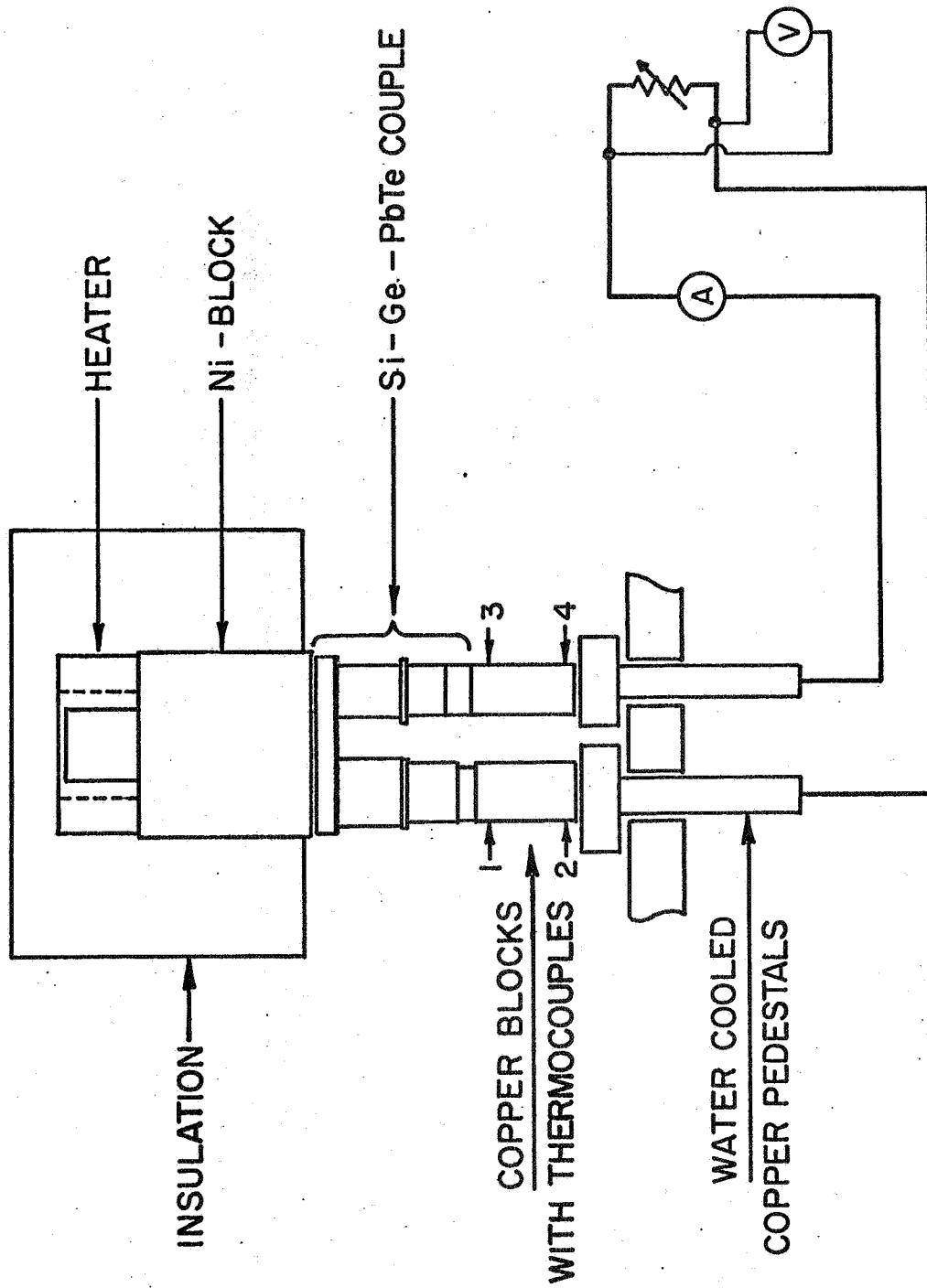
Fig. 7   Schematic diagram of apparatus for measurement
of conversion efficiency.

is approximately 0.55 inches, while the cross-sectional areas of the blocks are slightly larger than the areas of the corresponding legs. A heat flow of approximately 15 watts gives a temperature difference of approximately 4°C. The copper blocks are not attached to the water-cooled copper pedestals since the spacing between the thermocouple legs can vary; an Hg-In-Tl alloy, liquid at room temperature, is used in this joint to provide good thermal and electrical contact. A small amount of this material is also used in the junction between the copper blocks and the copper cold shoes of the couples.

The water-cooled copper pedestals serve as feed-throughs for the current leads which are of heavy welding cable. The measurement circuit consists of an ammeter in series in the circuit, a millivoltmeter connected across the circuit, and a twelve position high-current rotary switch which serves to vary the load resistance from approximately 4 mΩ. This is shown schematically in Fig. 7.

The measurement procedures are quite straightforward. The heater power is brought to the level which will give approximately the desired hot junction temperature. A thermocouple embedded in the lower part of the Ni- block indicates when temperature equilibrium is reached. The couple is allowed to come to equilibrium at some value of the load resistance. Then the various thermocouples are read, the values of load current and voltage recorded, and the open circuit measured by opening the circuit and reading the voltage immediately. These measurements suffice to calculate the following quantities:

$$\text{Power:} \quad P = I \cdot V_{load} + I^2 \cdot R_c$$

$$\text{Internal Resistance:} \quad R_i = \frac{V_{o.c.} - V_{load}}{I} - R_c$$

$$\text{Heat flux:} \quad Q = \Delta T_H \cdot K_N + \Delta T_p \cdot K_p$$

$$\text{Efficiency:} \quad \epsilon = \frac{P}{Q + P}$$

A correction factor, to account for the resistance of the leads R_c, is inserted in the equations for power and internal resistance. The constants K_n and K_p are calculated from the geometry of the copper blocks and their conductivity. The temperature of the hot junctions is measured with a micro-optical pyrometer focused at the junctions.

The measurement of the cold end heat flux by the technique described above is subject to the same errors as are most thermal conductivity measurements at low temperatures. In this case errors which decrease the measured ΔT tend to increase the calculated efficiency, while the opposite will occur with errors which increase ΔT. The thermocouples were selected to measure a single temperature within the precision of the potentiometer (0.01°C). Thus the error arising from inherent thermocouple differences would be a maximum of approximately 1% in the measured Q. Repeated measurements of a single heat flux showed a precision of approximately 2% in a number of tests. A more important source of error, and more difficult to assess, arises from thermal resistances in the solder joints and copper-to-copper contacts of the cold ends of the couples.

These losses do exist and they are in the direction which gives an increased efficiency; however, their exact assessment would be extremely difficult. As a result, five percent was added to all measured heat fluxes, to compensate for these losses. This value is somewhat arbitrary but is felt to be fairly realistic.

One check on the over-all applicability of this measurement technique was achieved by comparing the heat flux under closed circuit conditions with the calculated conduction heat through the couple. For example, at 800°C the calculated conduction heat is approximately 23 watts, while the measured conduction heat is approximately 24 watts.

C. Results

The results of measurements on these couples are summarized in Table III. Measurement have been made so far only at the nominal 50° cold junction temperature.

The current-voltage relationships are shown in Fig. 8; curves are shown for the actual and predicted performance at a hot junction temperature of 800°. The measured operating efficiency, was 96% of the predicted efficiency. The power output was 87% of that predicted. This seems to be the result of the open circuit voltage being slightly low. In fact the performance predicted for 800° was more closely achieved at 850°, which is apparently the result of the properties of the materials incorporated in the couples being slightly different from those used in calculating the performance of the couple.

The W-Si-Ge contact has an extremely short lifetime at temperatures above 700°C. This proved to be an experimental difficulty in that the resistance of most couples tested increased with time at 800°C or higher. Thus in a number of cases, the measured efficiency of couples with degrading hot junctions was decreased by 15 to 20%.

Stable, high temperature contacts between Si-Ge alloys and metal silicide hot straps have been developed by the Radio Corporation of America and by Siemens-Schuckertwerke, AG in West Germany, so that this is not a fundamental difficulty in the use of these materials.

The power density of the experimental couples is 1.20 watts/ cm^2, and the power-to-weight ratio is 72 watts/pound, for the thermoelectric materials alone. The over-all size of these couples could certainly be reduced by fifty percent without incurring any problems. This would increase the power density to 2.4 watts/cm^2, which is equivalent to approximately 2.2 Kw/ft^2. The power-to-weight ratio of a couple one-half the size of the experimental couples, with the appropriate intermediate and hot side contacts, could be expected to be approximately 105 watts/pound.
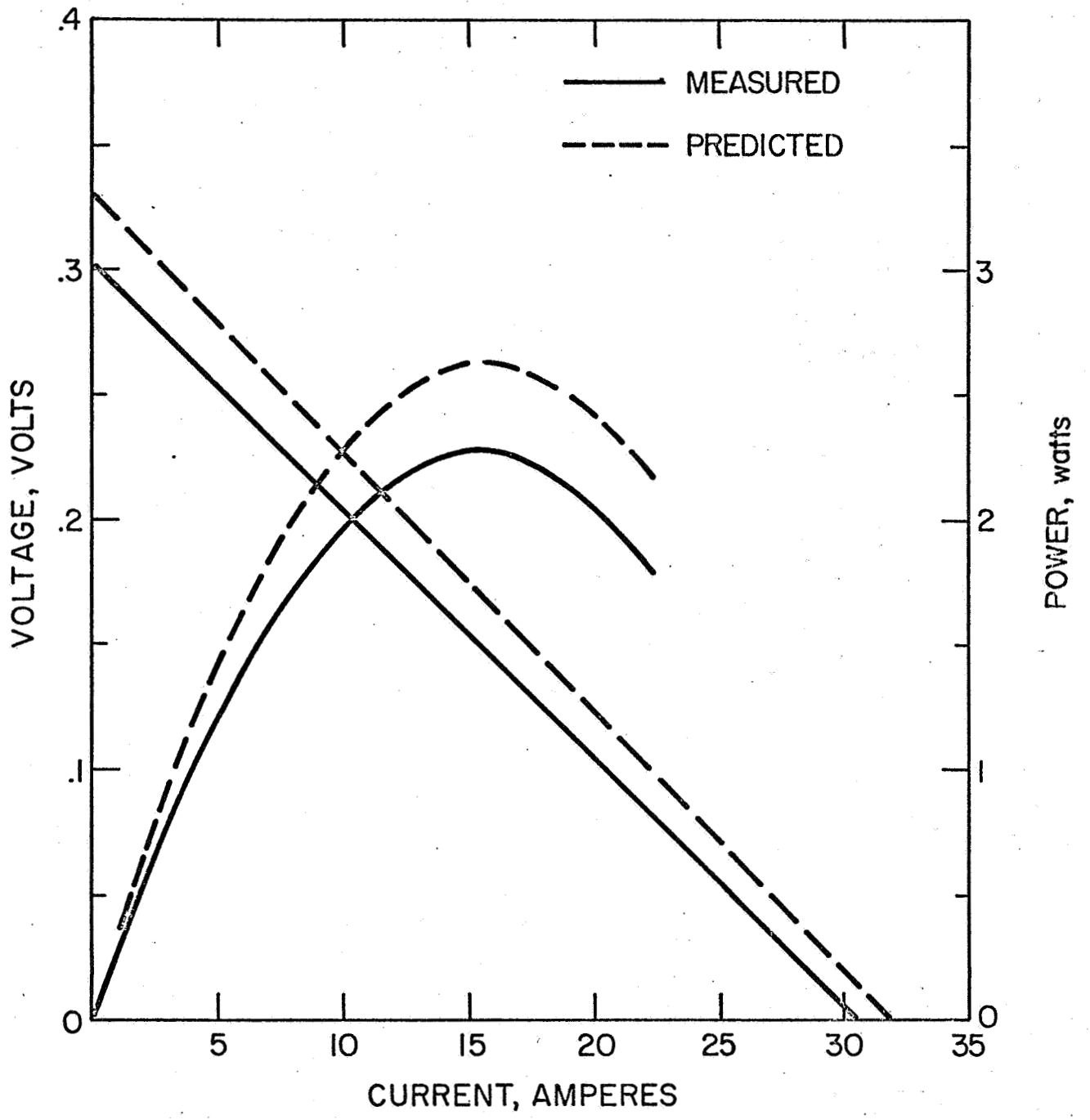
Fig. 8 Calculated and measured current-voltage-power relationships for Si-Ge-PbTe operating between 800° and 55°C.

TABLE III

Measured Performance of Segmented Si-Ge-PbTe

T_H	T_C	R_I	V_{oc}	P_{max}	Efficiency
°C	°C	m Ω	mv	watts	%
700	46	8.80	240	1.64	7.3
750	50	9.35	270	1.95	7.9
800	52	9.90	300	2.28	8.7
850	55	10.40	330	2.62	8.6
900	57	10.85	350	2.82	8.5

IV. PORE MIGRATION IN SINTERED PbTe-SnTe THERMOELECTRIC ELEMENTS

A. Introduction

The combination of high vapor pressure, extensive internal porosity, and operation in a temperature gradient makes pore migration a possible degradation mechanism in pressed-and-sintered PbTe thermoelectric elements. Pores will migrate up the temperature gradient, eventually bringing them to the hot end contact. Sufficient numbers of pores at the hot junction would cause a highly resistive contact or even physical separation of the contact. Such occurrences would probably require rather long times, since a number of mechanisms can operate to counteract the wholesale migration of pores. However, the long times which are currently envisioned for operation of thermoelectric generators (25,000 to 40,000 hours) require serious consideration of even the slowest degradation mechanisms.

A pore in PbTe will migrate in a temperature gradient by vapor transport of material from the hot side of the pore to the cold side. A simple equation can be developed for the instantaneous rate of migration, or velocity, of a given pore which is given by

$$V_x = \frac{2r \cdot \left(\frac{dS}{dT}\right)_{Tx} \cdot \left(\frac{dT}{dX}\right)_x}{\rho}$$

where r is the radius of the pore; $(dS/dT)_{Tx}$ is the slope of the sublimation rate versus temperature relation at T_x, the temperature of the midpoint of the pore; $(dT/dX)_x$ is the temperature gradient at the pore; and ρ is the density of the pure material. Since the derivative of the sublimation rate vs. temperature is positive, a given pore will accelerate as the pore migrates up the temperature gradient. (The equation of motion of a migrating pore should be the same as that for a charged particle moving freely toward an oppositely charged electrode.) The equation above also predicts dependence of migration velocity on the radius of the pore. Figure 9 shows a set of curves of migration rate as a function of temperature calculated
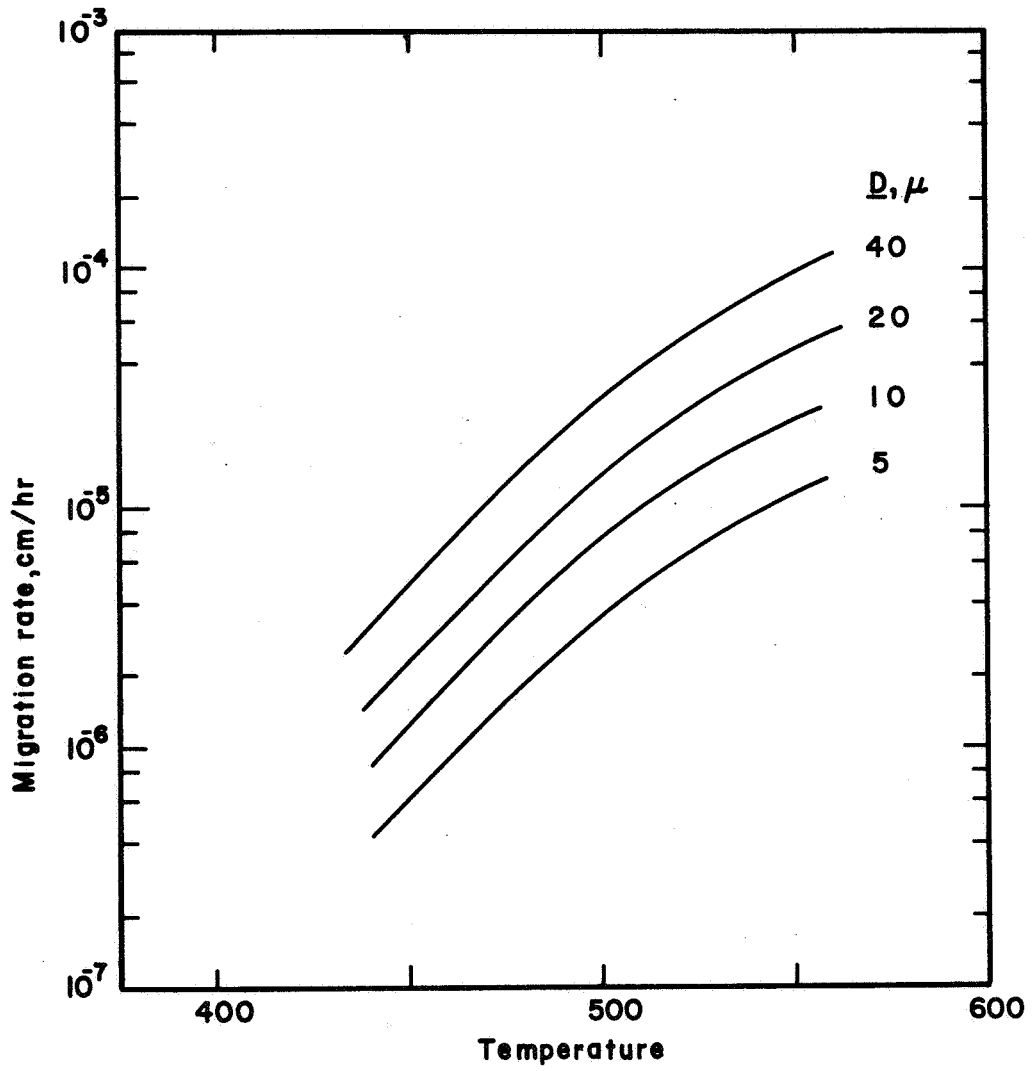
Fig. 9 Calculated migration rate as a function of temperature for four pore sizes.

from equation (3), assuming a temperature gradient of 500°C/cm, for three pore sizes. These curves are based on sublimation rate measurements made in vacuum on 3P elements. [17]

Rough calculations based on our knowledge of the volume fraction of pores and average pore diameter in 3P materials and on the calculated migration velocities above indicate that migrating pores could destroy a significant fraction (such as one third) of the area of a contact at 525°C within times of the order of 10,000 hours. These predictions should be modified considerably for real materials, however. Instead of every pore being able to move freely for the entire length of the element, in real materials many pores are already pinned at grain boundaries and the availability of grain boundaries and second phase particles and foreign inclusions should serve to trap many more which might be free to migrate initially. This has been shown to occur on a finer scale than that considered here by Ashbee[18] who observed migration and trapping of pores in UO_2 foils heated in an electron microscope beam. Almost any discontinuity in the structure, including dislocations, which lowers the total surface energy of a pore will impede its further motion.

B. Experimental Procedures

Preliminary investigations into the occurrence of pore migration in real thermoelements have been made by quantitative metallography on gradient tested 3P elements. Five elements were examined. These had operated 3850 hours at a hot junction temperature of 510°C and cold junction temperature of approximately 60°C. The elements were approximately 0.245 inches long. Five samples from the same purchase lots of material and bonding runs, but with no gradient history, were used as controls. All samples were mounted, sectioned lengthwise on a diameter, and lightly polished and etched. Photomicrographs were taken at 45 X along the lengths of the elements. These photomicrographs were then divided into two so that the length was divided into eight sections,

each representing approximately 0.030 inches of actual length on the element. The area covered by the photomicrographs was approximately 0.245 by 0.090 inches. The pores were counted from the photomicrographs using a Zeiss particle size analyzer.

The data were treated in the following manner: The first seven poresize categories were summed and averaged for the eight length intervals. The midpoint of each interval was taken as the representative distance from the hot end. Approximately ninety percent of the pores counted fell in this range of sizes.

The frequency distribution of the first twelve pore size categories was also calculated and plotted. The basic assumption used in treating the data was that a fairly uniform distribution of pores exists in any sample of as-bonded or new elements. This distribution should be different in an element which has been held in a gradient for a sufficiently long period (if migration of pores does occur). This is illustrated schematically in Fig. 10. The upper curve represents the hypothetical normal distribution of a given size (or sizes) pf pores, while the middle curve represents a possible distribution to be found after pores migrated toward a hot end at the right. At some point, as shown, the number of pores should decrease below the average level since the rate of supply from the left is much lower, due to the lower temperature, than the rate of migration to the right. Depending upon the length of time for migration, the level would rise above the average value initially at some point, as shown, the number of pores should decrease below the average level since the rate of supply from the left is much lower, due to the lower temperature, than the rate of migration to the right. Depending upon the length of time for migration, the level would rise above the average value initially at some point near the hot end then gradually decrease to a form such as is shown in the lowest curve. This should by typical of the steady-state distribution after migration of a significant number of pores to the hot end.
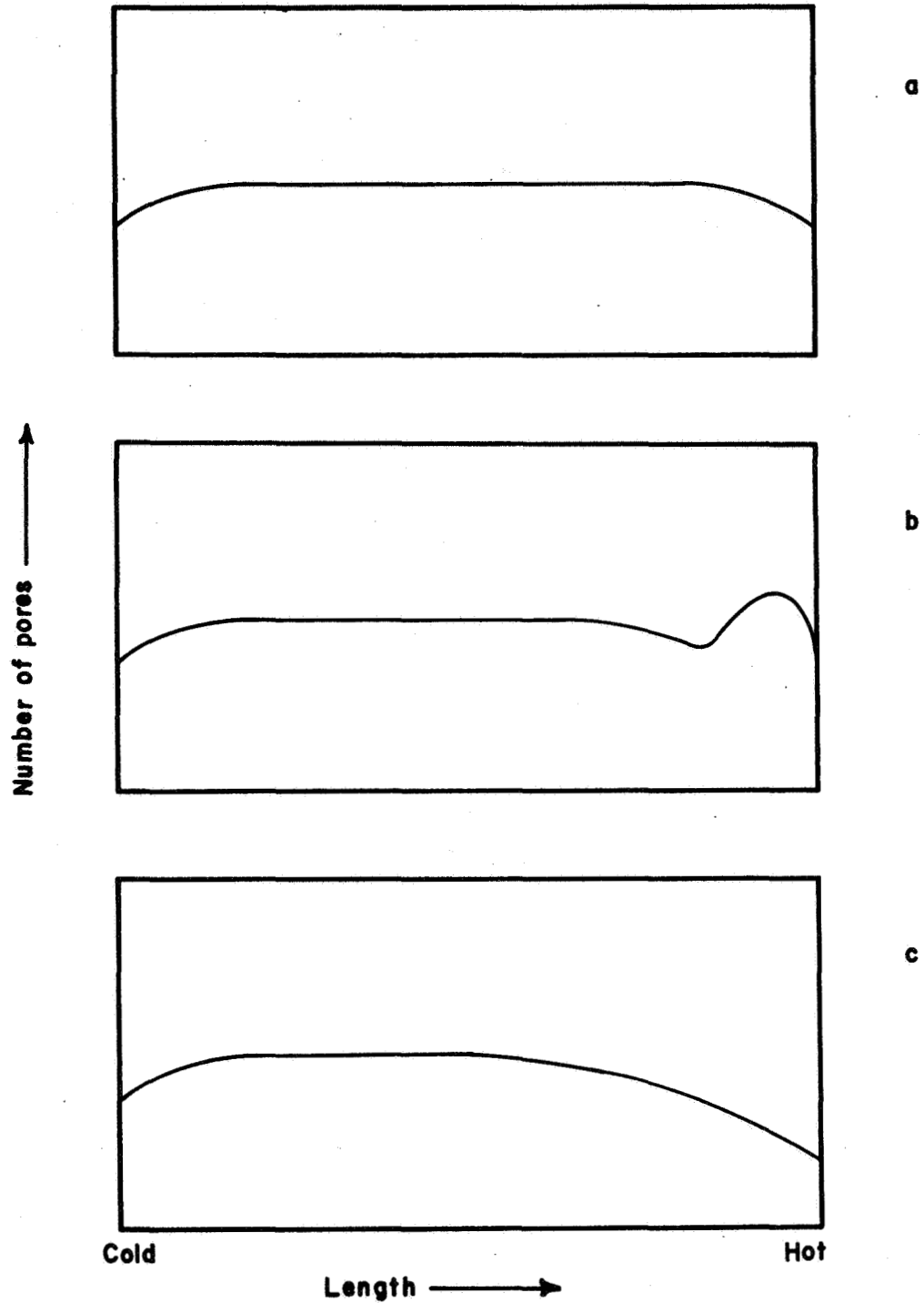
Fig. 10 Schematic curves illustrating the distribution
of pores over the length of an element held in
a gradient at a) zero time b) after initial migration
c) steady-state distribution after extended
operation.

C. Results

Figure 11 shows the variation of average pore frequency per unit area over the length of the control elements. The over-all shape is essentially what one would expect from a powder compact pressed in a double-action die. The ends of such a compact are more dense than the middle. The dip in pore frequency in the middle is probably indicative of the scatter possible with the small number of specimens making up the average, rather than of a significant variation in pore frequency.

Figure 12 shows the variation in pore frequency along the length of the elements held 3850 hours in a gradient. The hot end is at the origin. The average number of pores at the hot end is substantially different from the control elements (and from the cold end of the tested elements). The differences appear to be large enough and in the expected directions to provide reasonable assurance that actual migration has occurred to produce this distribution. Variations in the data have very probably contributed to the over-all configuration, as will be shown below.

The average pore size in 3P material is approximately 25 microns; (the majority of pores fall fairly close to this size as well, as can be seen from Figs. 13 and 14). Calculations from the conditions of the gradient life test show that pores starting from positions with an average temperature of 500°, 450°, and 400° would move 40, 6.5, 0.7 thousandths of an inch, respectively, in 3850 hours. The actual distances would be greater because of acceleration in moving into regions of higher temperature. The approximate positions at which these temperatures occur are indicated in Fig. 12. It is fairly clear that the pronounced dip in the area of 90 mils cannot be the result of depletion of pores by migration. However, the shape of the distribution within the first 50 mils can very probably be attributed to migration of pores, since the temperatures encountered have been shown to be able to produce migration distances of from approximately 5 to 35 microns.
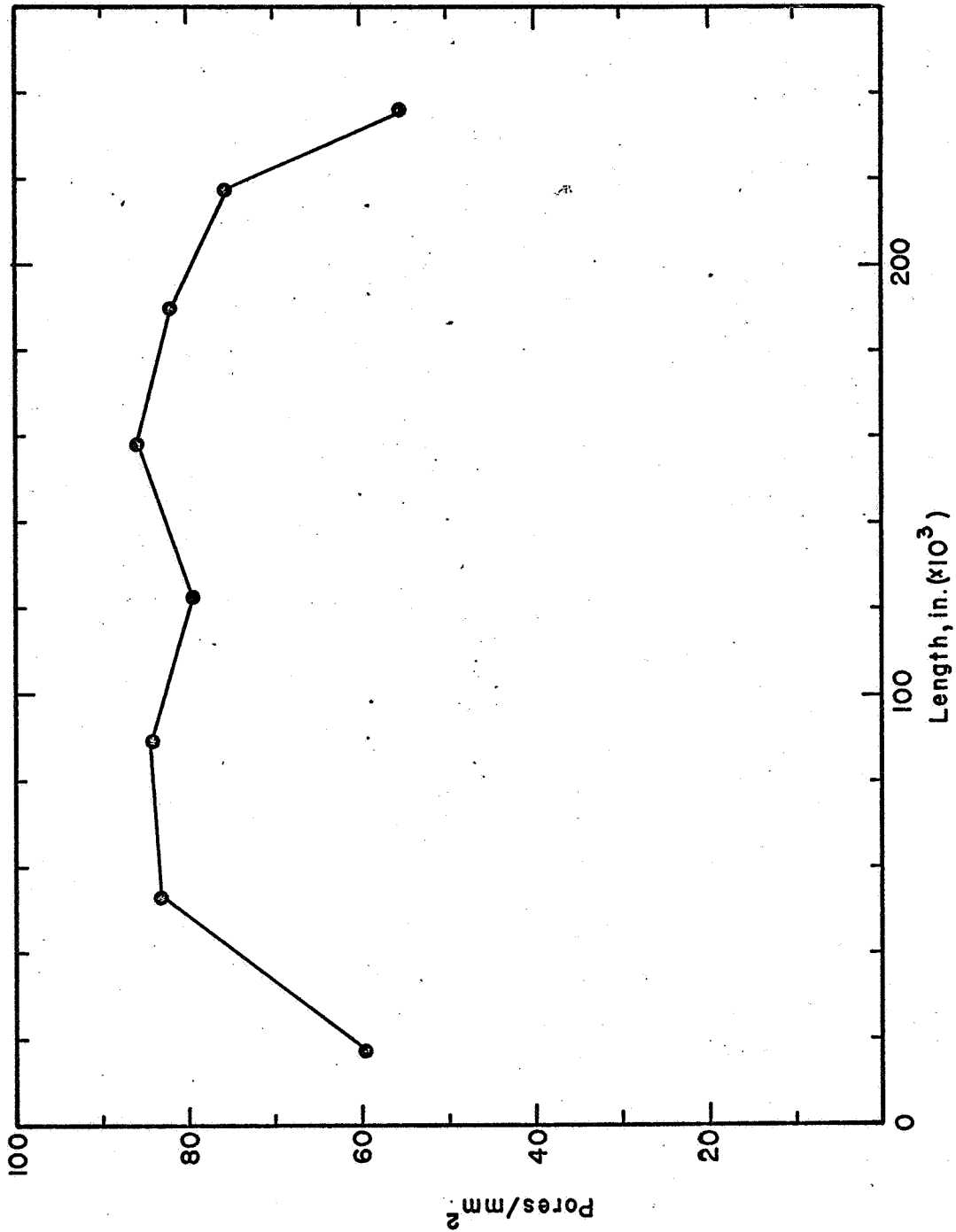
Fig. 11 Distribution of pores as a function of length in
as-bonded elements. Includes pores from 10-35
microns in diameter.

Fig. 12 Distribution of pores as a function of length in gradient-tested elements, held 3850 hours at $T_H = 510°$, $T_C = 60°C$, hot end at left.
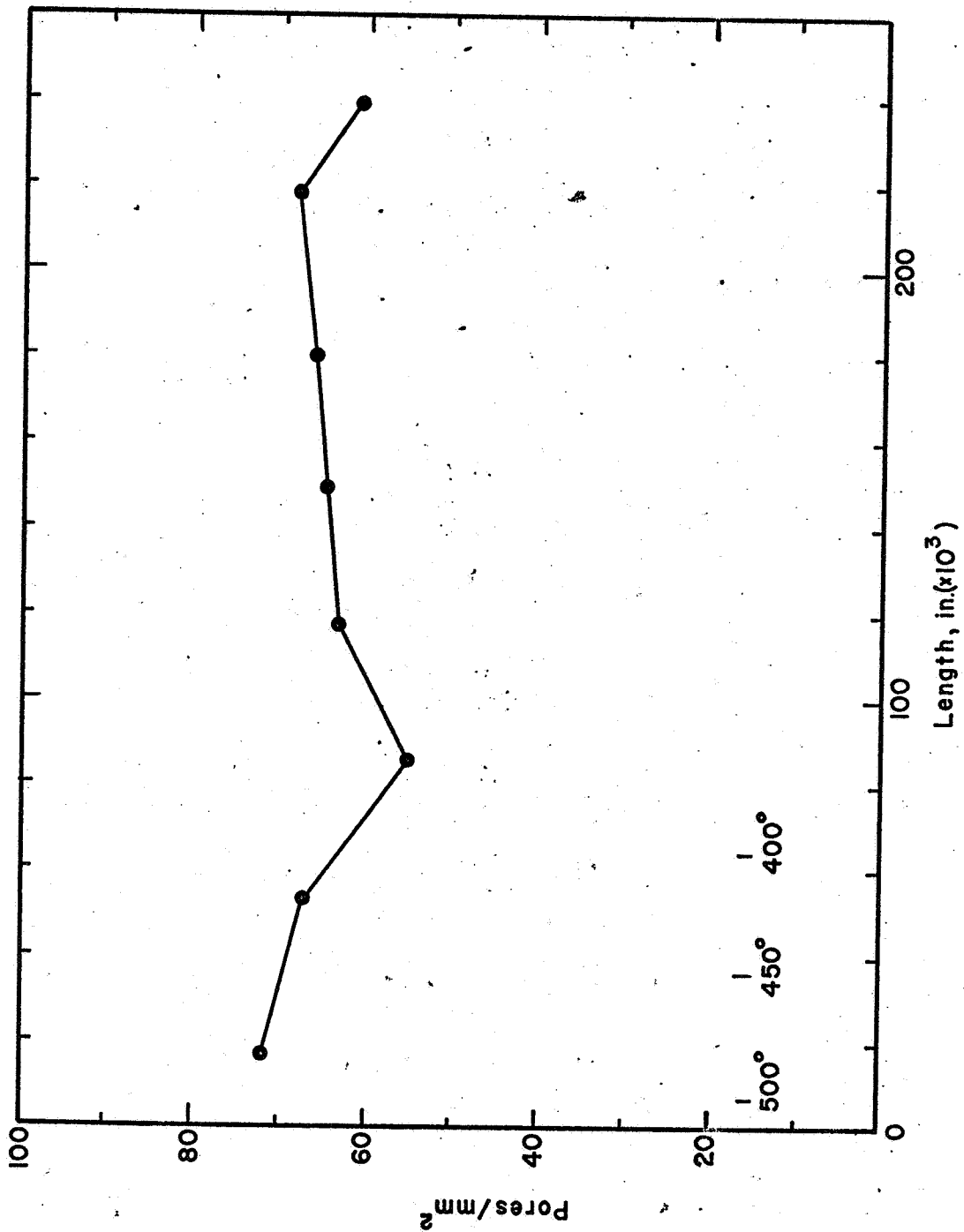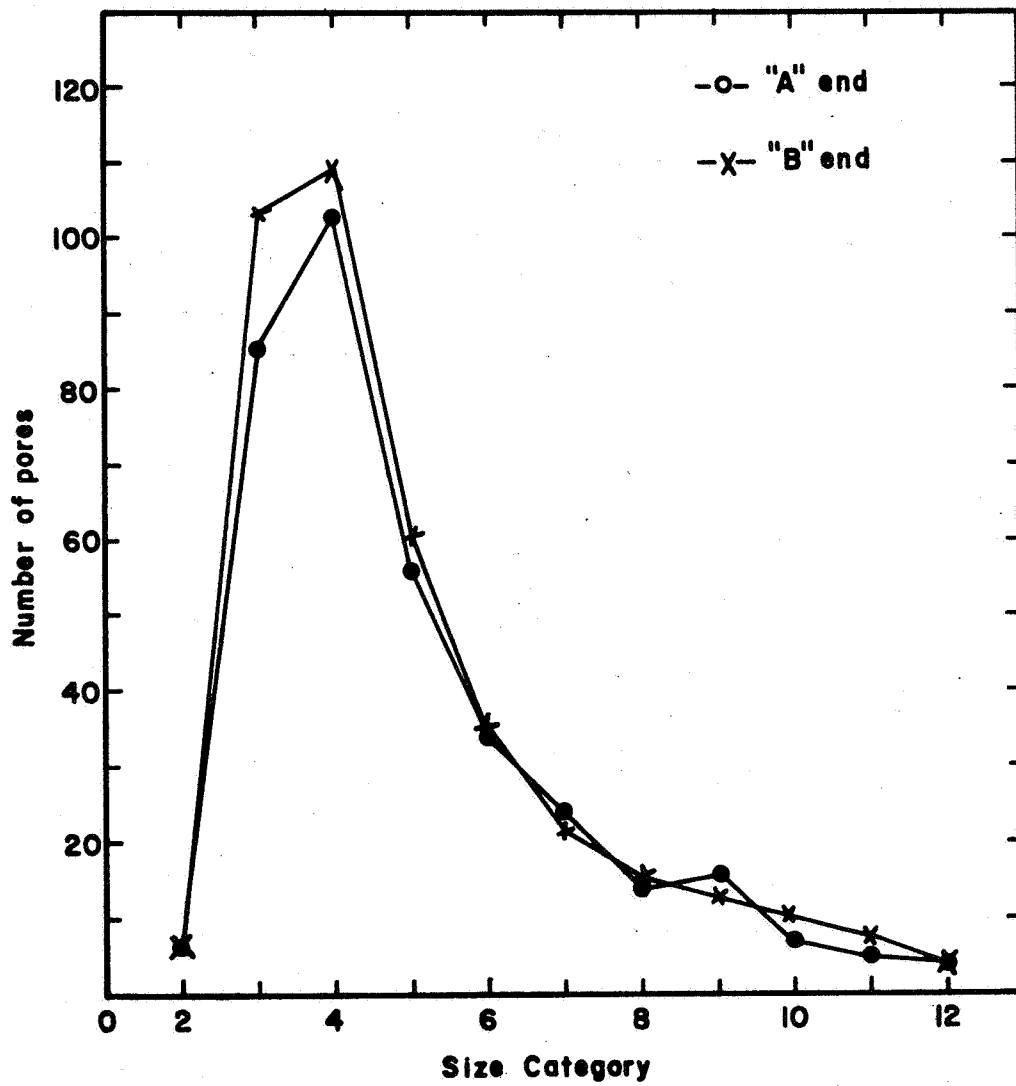
Fig. 13 Frequency distribution of pores at opposite ends of as-bonded elements; includes pores from 10 - 55 microns in diameter.
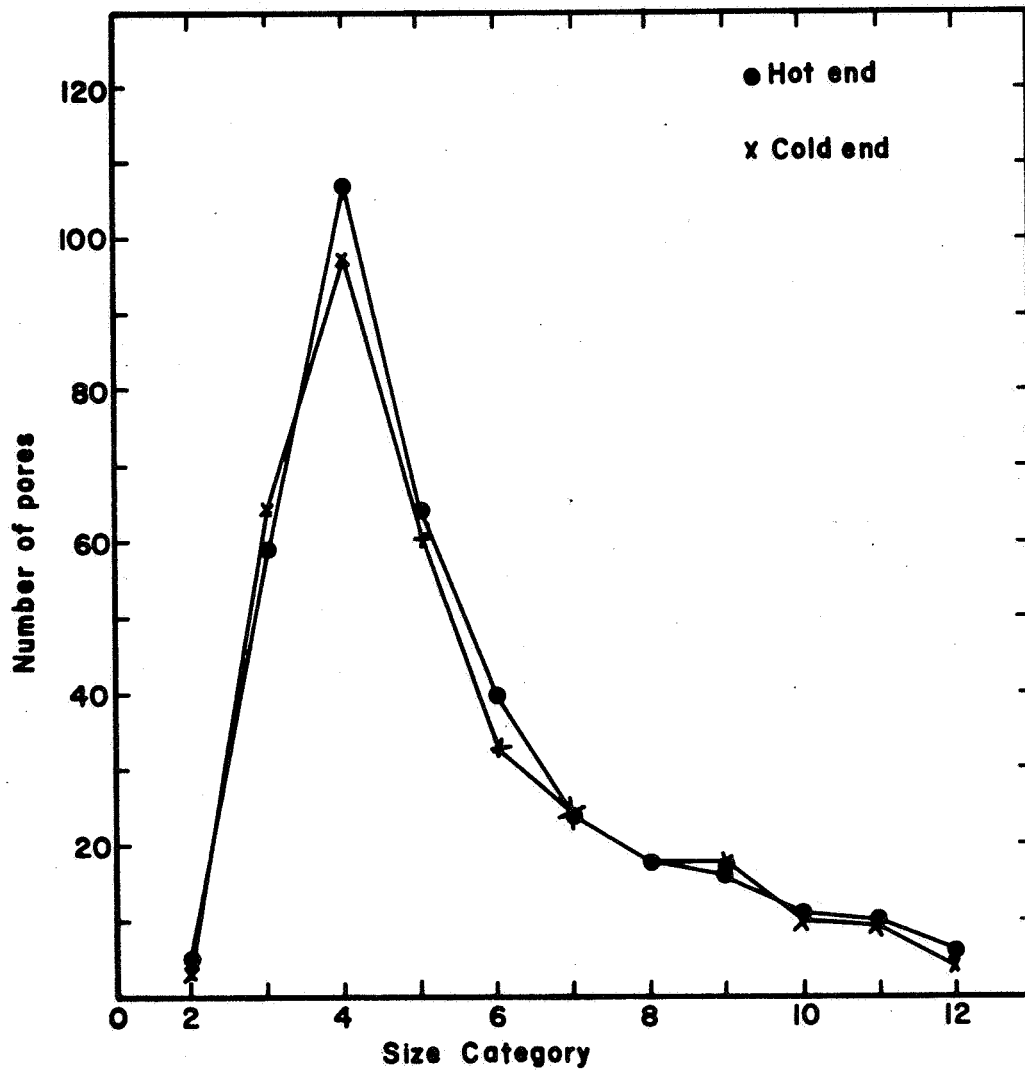
Fig. 14 Frequency distribution of pores at hot end cold
ends of gradient-tested elements; includes pores
from 10 - 55 microns in diameter.

The frequency distribution of the first twelve pore sizes are shown in Figs. 13 and 14 for as bonded and gradient-tested elements, respectively. The size categories and the actual pore diameters they represent are listed in Table IV.

The distribution curves relate to the number of pores counted in an actual area of 4.28 mm^2. There are no striking differences between either the control and gradient-tested elements or between the hot and cold ends of the gradient-tested elements. The latter makes it impossible to test the prediction of size dependence of the migration rate. If larger pores do indeed migrate faster, the distribution curve from the hot end should show some higher frequencies for the larger sizes. A similar effect would be observed if smaller pores coalesced; thus the change in the size distribution curve is not conclusive evidence for radius dependence of migration rate. The problem arises mainly from the small number of observations which make the detection of small statistical effects very risky considering the low precision of a small sample. It is for this reason that we hesitate, without increasing the number of observations, to say more than that there appears to have been migration of enough pores to be detected by the technique used. It was also rather unexpected to find such an apparently sizeable migration of pores considering the microstructure of the 3P material which seems to present such an abundance of various traps for freely moving pores.

We hope to be able to make more measurements in order to increase our certainty on the effect found here, for we feel that this could have important consequences for all bonded PbTe structures.

TABLE IV

Actual Median Diameters of Pore Size Categories
Measured

Size Category	Pore Diameter, microns
1	0 - 11. 1
2	15. 1
3	19. 1
4	23. 1
5	27. 1
6	31. 1
7	35. 1
8	39. 1
9	43. 1
10	47. 1
11	51. 1
12	55. 1

V. LIFE TESTING

A. Isothermal Tests

The results of a series of isothermal tests at 525°C on W-bonded 3P elements were reported in the Second Interim Summary Report. These were tests of batches of elements held at temperature for 1000, 2000, and 3000 hours. After measurement, these three groups of elements were put back on test at 525°C.

The group of elements originally measured at 2000 hours was removed after another 2000 hours. The furnace was found to be operating at 740°, due to a malfunction of the controller. The test had been running at this temperature for at most 1000 hours; however, the elements had all lost greater or lesser amounts of material by vapor transport, rendering them unfit for further analysis.

The group of elements which was tested at 3000 hours originally was tested for another 3000 hours. The results of measurements after a total of 6000 hours at 525°C are reported below. Table V lists the values of contact and element resistances at 3000 and 6000 hours for these elements. Five contacts, out of ten tested for the second 3000 hours, remained intact, although only three could be measured. The average values of element and contact resistances and Seebeck voltage are listed in Table VI. The over-all averages and average values calculated for just those elements and bonds still measurable at 6000 hours are both given.

The contact resistance of the measurable bonds remaining at 6000 hours has increased five-fold from 60 to 300 μ Ω (19 to 95 μ Ω - cm^2). The element resistance has decreased slightly after a fairly large increase in the first 3000 hours of testing. A slight decrease in Seebeck voltage, initially, has been followed by an increase. The over-all increase in Seebeck voltage is only about 2.5%.

The most significant cause of degradation of the elements seems to have been cracking. Six elements out of fourteen have fractured, and indeed the increased resistance may be largely due

TABLE V

Contact and Element Resistances of W-Bonded 3P Elements
Tested 6000 hours at 525°C

| Element | 3000 Hours | | | 6000 Hours | | |
	Top CR	Bottom CR	Element	Top CR	Bottom CR	Element
	$\mu\,\Omega$	$\mu\,\Omega$	$m\,\Omega$	$\mu\,\Omega$	$\mu\,\Omega$	$m\,\Omega$
3M6P21	*	320	2.98	n.r.	*	2.00
5O4P21	--	---	2.08	n.r.	n.r.	n.r.
5O1P21	*	---	1.98	n.r.	n.r.	n.r.
5O6P21	1115	75	2.70	---	---	*
5O2P21	--	255	2.08	---	---	2.05
5O8P21	--	190	1.94	---	---	1.85
5O9P21	--	---	1.94	n.r.	n.r.	n.r.
5Q1P21	--	120	2.50	---	---	1.70
5Q9P21	80	---	2.28	*	---	*
5D7P19	85	---	2.08	375	---	1.88
5D8P19	*	---	6.0*	n.r.	n.r.	n.r.
5D4P19	60	---	1.53	340	---	1.71
5C3P19	--	80	1.10	---	180	1.80
4Y13P19	--	150	1.53	---	---	2.11

n.r.   not run

*   cracked element, bond intact but not measurable.

---   bond failed

TABLE VI

Summary of Average Properties of W-Bonded 3P Elements
Tested 6000 hrs. at 525°C

	0 hrs.	3000 hrs.	6000 hrs.
Element resistance, over-all, mΩ	1.57	2.05	1.89
Element resistance, 8 elements, mΩ	1.53	1.96	1.89
Contact resistance, over-all, $\mu\Omega$	60	140	300
Contact resistance, 3 bonds, $\mu\Omega$	60	75	300
Seebeck voltage, 500° vs. Cu, mv	74	73	76
Number of elements intact	14	13	8
Number of bonds intact	23	13	5

to microcracking. In comparing this result to the gradient test (section IV), it appears that the isothermal test is a more severe test of mechanical stability. While cracking was widespread in the gradient tested elements, none failed, either by large increases in resistance (such as 5 times) or by mechanical collapse. Apparently, the compressive loading maintains fairly good electrical resistance, even across numerous cracks. Fracturing of the isothermal elements takes a rather diverse course as shown in the accompanying photograph, Fig. 15. There seems to be a general tendency toward diagonal fractures through the element which then turn more nearly transverse as the fracture nears the bond to an electrode (although, of course, the actual sequence may proceed in the opposite direction). Whatever the cause or sequence of events in cracking of these elements (and it is not an isolated instance), it gives a strong indication that compressive loading is a desirable feature to retain in a generator structure, regardless of the type of contact employed.

The third group of elements, originally measured at 1000 hours, remains on test at this writing. An additional 4650 hours have been accumulated. These elements will be measured after a total of approximately 7000 hours has been reached.

Another group of elements has been prepared for testing. Their initial properties are listed in Table VII. This test has been set up, in part, to examine further the possibility that significant differences in behavior exist between different lots of material and also to test the possibility of predicting the long-term performance of bonded elements from the results of a fairly short test. Thus, these elements will be tested for approximately 1500 hours, then put back on test after measurement.

B. Couple Life Testing

The design and construction of a sixteen station device for life testing of bonded and unbonded thermoelectric couples was described in the Second Interim Summary Report. The results of the first test with this device are reported in this section.
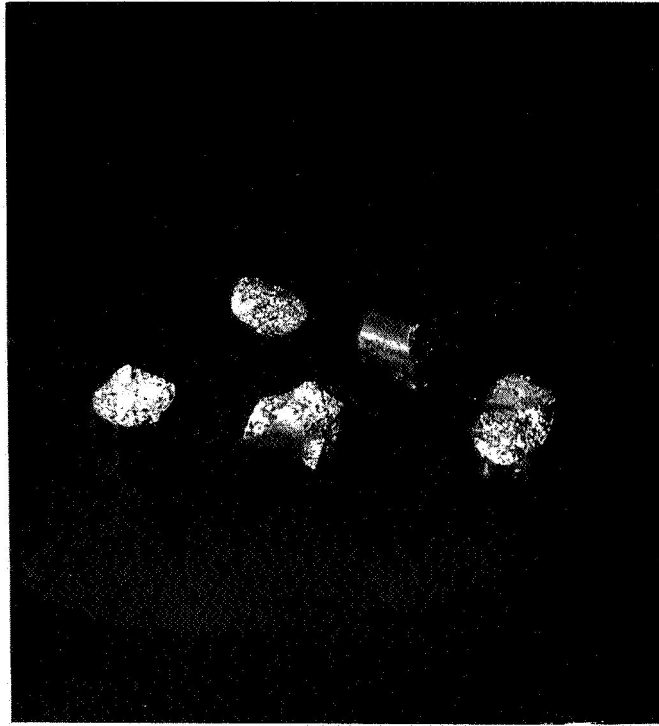
Fig. 15 Macrophotograph of fractured elements and their electrodes. Elements isothermally tested 6000 hours at 525°C; total number of temperature cycles approximately seven.

TABLE VII

Initial Properties of W-Bonded 3P Elements
To Be Tested Isothermally

Element	C.R. T $\mu \Omega$	C.R. B $\mu \Omega$	Element m Ω	Seebeck Voltage (500° vs. Cu) mv
7I9 P37	100	80	1.81	
7I7 P37	125	70	1.87	
7I13 P37	50	100	1.87	68
7I8 P37	100	50	1.85	
7I14 P37	105	135	1.69	70
7I15 P37	180	60	1.73	70
7I15 P37	175	200	1.78	
7I2 P37	-	80	1.87	
7H8 P33A	105	70	1.85	67
7H15 P33A	-	60	1.96	64
7H18 P33A	150	150	2.05	68
7H17 P33A	-	80	2.13	
31 P37			2.19	70
34 P37			1.95	69
35 P37			1.96	70
3 P33A			2.01	71
4 P33A			1.85	70
5 P33A			1.92	70

x   Indicates cracked or broken element, but intact bond.

-   Failed or initially missing contact.

1. PbTe Couple Test No. 1

The loading for this test consisted of fourteen 3N-3P couples bonded to common tungsten hot straps, and two 3N-3P couples pressure contacted to tungsten hot straps. The average value of the room temperature resistance for the bonded couples, with copper cold shoes, was 3.275 mΩ. The initial performance of all couples in this test is listed in Table VIII. As was noted previously, the open circuit voltage and total resistance are lower than predicted. This is apparently the result of the indicated hot strap temperature's being higher than the actual junction temperature—although it would also seem that the deficiency in Seebeck voltage is such that the Seebeck coefficients of the materials are probably lower than the published average values used in calculating the performance of the couples.

The tester was operated on manual control for the first two weeks of the test. During this time it was noted that considerable oxidation of the tungsten hot straps and hot portions of the couple legs was occurring. This was felt to be a result of continued water evolution from the heater insulators. The system was therefore pumped and backfilled twice while operating. Since the heat transfer characteristics of the heaters are highly variable with the pressure of the tester atmosphere, this required fairly delicate manipulation of the power input as the bell jar was evacuated. This seemed to diminish the progress of the oxidation of the couples.

When control was switched to the automatic temperature controller, it was found to operate erratically, cycling the temperature up and down over almost the entire range in an unpredictable fashion. During the time and tests required to locate and correct this problem, the tester was run continuously, and the test couples were subjected to an undetermined number of temperature cycles of great rapidity. The small thermal mass of the individual heaters allows them to heat and cool at rates on the order of 400° - 500°C per minute. The number of cycles of the tester during repair of the controller can

TABLE VIII

Couple Life Test I - Initial Operating Parameters

Couple	Resistance	T_H °C	T_C °C	ΔT °C	Voc mv	R_I m Ω	P_{max} watts
6 R1	3.25	470	37	433	143	14.2	0.36
6 G2	305	470	37	433	140	10.6	0.463
6 G3	3.25	520	37	483	156	12.7	0.478
6 W1	3.45	490	37	453	152	15.2	0.38
6 W2	3.40	540	36	504	159	15.8	0.40
6 W3	3.35	480	40	440	141	13.2	0.377
6 Y5	3.40	480	36	444	155	11.5	0.522
6 Y8	3.30	500	36	464	155	10.3	0.585
#1 Unbonded		550	38	512	163	52	0.130
6 Z1	3.30	470	37	433	157	11.4	0.540
6 Z2	3.20	490	36	454	155	11.0	0.545
6 Z5	3.45	460	38	422	141	9.9	0.560
6 Z6	3.15	490	35	455	163	11.9	0.560
6 Z7	3.20	460	35	425	138	10.9	0.435
6 Z8	3.00	520	38	482	159	14.4	0.440
#2 Unbonded		520	36	484	152	37	0.156
Average values:		495	36	456	151	11	

convervatively be placed at 30 to 35. No data were taken during this period, which is indicated by the broken lines in Fig. 16. For a number of couples the internal resistance increased tremendously as an apparent result of the temperature cycling. Some couples were largely unaffected, however; their performance is discussed in the following paragraphs. The test was discontinued after 800 hours since it was felt that too few couples were left to produce meaningful results.

Six couples remained low in resistance after the repair of the heater control. The exact reason for the superior performance of these couples compared with the others is not entirely clear. Their initial room temperature resistance was slightly higher than average at 3.285 mΩ. Initially, the average hot junction temperature of the six couples was 24° below that for the other eight bonded, 475° versus 499°. Subsequently, the difference in average hot junction temperature was only a few degrees. This is shown in Fig. 16, where the open points represent the average T_H for the high resistance couples.

The other curves of Fig. 16 show the average values of open circuit voltage, internal resistance, and matched load power for the six low resistance couples. (The solid points on these curves represent average values corrected to hot junction temperatures represented by solid points). The corrections were simple linear, with no account taken of the temperature variation in Seebeck coefficient or resistivity. This procedure was adequate except for the point at 50 hours. The general behavior of these couples, however, is fairly clear whichever data is used. During the first one hundred hours, the resistance and open circuit voltage decreased markedly. The decrease in resistance was great enough that an increase in power was achieved. There can be little doubt about the reality of this decrease, since at fifty hours, even with a very high hot junction tempera ture, the resistance (uncorrected) had decreased approximately 10%. The other eight bonded couples were also apparently decreasing in resistivity, since the uncorrected
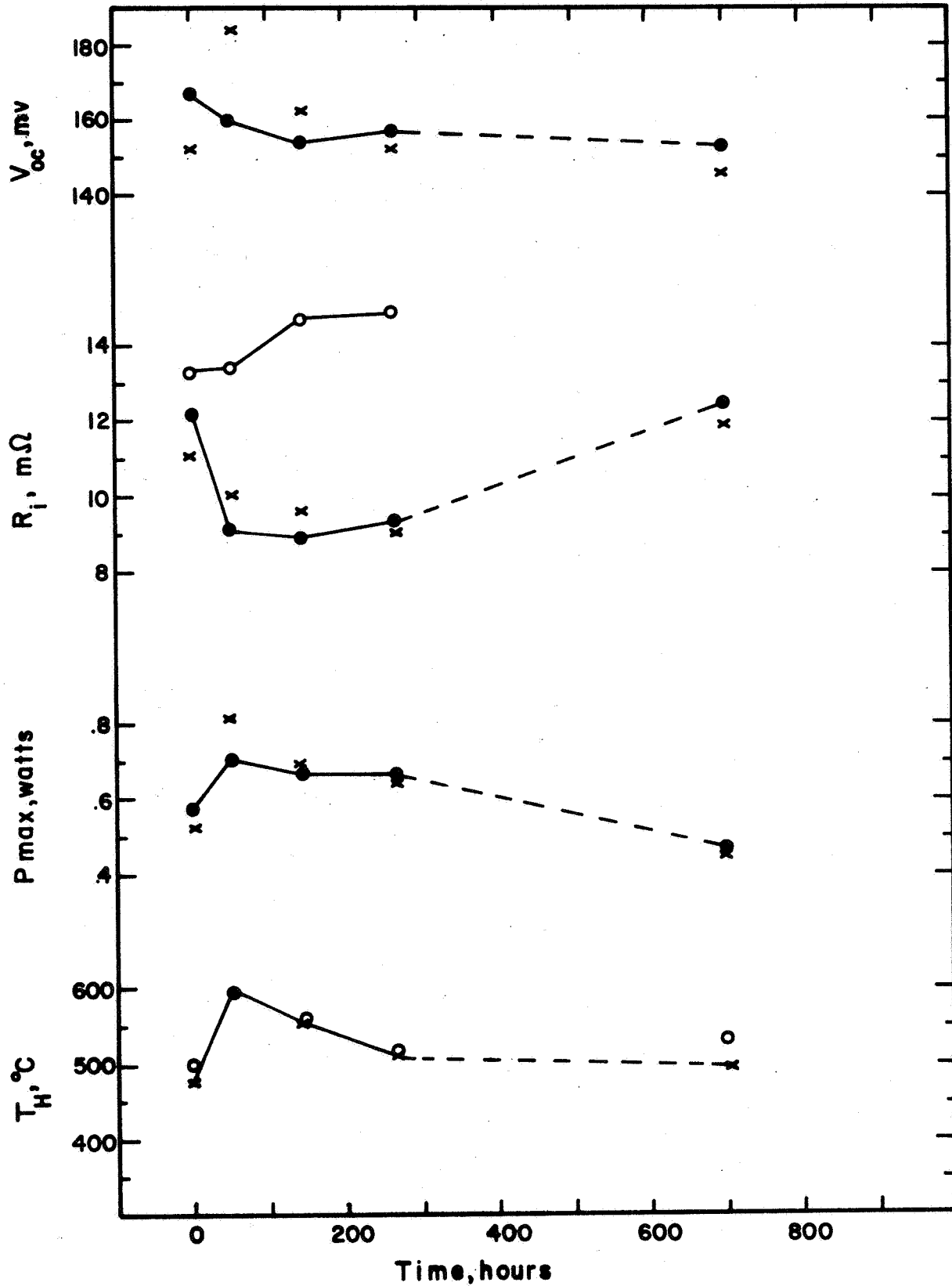
Fig. 16 Results of life test of fourteen W-bonded 3N-3P couples. Broken lines represent period of uncontrolled thermal cycling.

resistance changed from 13. 3 mΩ to 13. 4 in the face of a 100°
increase in hot junction temperature. This shown in Fig. 16 by the
curve through the open points for internal resistance. Thus, the
decrease in resistance was apparently a general phenomenon; it
simply happened to a greater extent in the low resistance elements.

Only one significant difference could be established from
prior information about the couples in this test. All but two couples
were prepared from the same purchase lots of material. However,
five of the six low resistance elements came from the same bonding
run and all had excellent bond resistances. The average bond
resistances of the low couples were 40 $\mu\Omega$ and 65 $\mu\Omega$ for p and n,
respectively. For the other eight couples, the corresponding
resistances were 110 $\mu\Omega$ and 85 $\mu\Omega$. Other variations in resistance
obscured the 0. 090 mΩ differences in contact resistance values.
It would appear from this that the superior performance of these
couples can be related to their excellent bond resistances. This
is contrary to the picture which has been emerging from other
tests. Most other results have indicated, contrary in this case to
expectation, that low bond resistances were not necessarily either
necessary or sufficient for stable resistance behavior. Perhaps
the significance of these couples is that for the conditions to which
they were subject a low resistance contact is the most stable.

This test suffered two setbacks in terms of its providing
meaningful data. The first was heavy oxidation of the hot straps
and upper portions of the tested couples. This was due to continued
release of water vapor from the refractory insulation of the heaters.
During the initial trials of the tester, considerable water had
evolved from the heaters (to the point of condensing on the bell jar);
however, the system was operated under vacuum at temperature
for several days to alleviate this problem. One difficulty here
was that operation in vacuum did not produce as high temperatures
in the heater insulation as did operation with an argon atmosphere.
Thus with the atmosphere present, higher temperatures are produced
in a greater volume of material, ultimately releasing more water
than is accessible to heating under vacuum.

The second was the unscheduled thermal cycling of the test couples. This was not a complete loss in that it gave the first indication that initial contact resistance is an indicator of subsequent performance under cycling conditions. This kind of correlation had not been evident from the accumulating results of isothermal testing.

2. PbTe Couple Test No. 2

During January a new batch of couples was loaded in preparation for another test. Table IX lists in the first column the initial resistances of these couples; in the second column, the resistance measured on the cold sinks with the couples in position; and in the third column, the contact (cold shoes to sink) resistance. Some couples were prewetted on the cold shoes with a liquid Hg-In-Tl alloy. These are denoted by an asterisk. The effect on the contact resistance is as variable as are the unwetted couples.

The couple tester was equipped with an internal desiccator for this test. A porous bottomed ceramic container was mounted on the gas inlet rube, such that the general circulation of the atmosphere within the bell jar should at least pass over the desiccant. The dissicant, P_2O_5, is arranged in alternating layers with thin sheets of quartz wool, within the container. Approximately 300 grams of P_2O_5 can be put into this device. The geometrical surface area exposed, that is the top layer, is approximatd y 110 cm^2; it is hoped that the arrangement as it stands will provide a greater effective area of desiccant. The equilibrium concentration of water vapor over P_2O_5 is approximately 2×10^{-5} mg H_2O per liter. We feel that the addition of this desiccant can significantly reduce the problem of water evolution from the heater refractories.

The test began on February 1, 1968 (at temperature), and is scheduled to continue indefinitely. The results will be reported in the future.

TABLE IX

Initial Room Temperature Resistance of
PbTe Couples - Life Test II

Couple	R $m \Omega$	R $m \Omega$	R_C $m \Omega$
7 E2 (Unbonded)	- - - -		
7 F8	3.25	3.70	0.45
766	3.55	3.88*	0.33
7F7	3.55	3.60*	0.05
7E1	3.10	3.60	0.50
764	3.42	3.58	0.16
7F6	3.45	3.58	0.13
7F2 (Unbonded)	- - - -		
765	3.30	3.50*	0.20
7F3	3.50	3.60	0.10
762	3.39	3.55	0.16
763	3.38	3.60*	0.22
7E4	3.42	3.50	0.08
7F1	3.58	3.60*	0.02
768	3.55	3.65	0.21
761	3.40	3.48*	0.08

* Cold contact wetted with Hg-In-Tl alloy.

C. Gradient Life Test IV

1. Results

The first 2600 hours of testing on a group of bonded and unbonded 3P elements were presented in the Second Interim Summary Report.

During this period, the test was interrupted for approximately a month, then continued until termination at 3850 hours. The additional 1250 hours of operation did not cause any substantial changes in the over-all picture of the test from that which existed at 2600 hours: the resistances of only three bonded elements and the three unbonded elements were still readable. The data have been replotted in Figs. 17, 18, and 19 to include the additional time on test.

Resistance values are shown for the unbonded elements and for three singly bonded elements which remained fairly low in resistance. Average Seebeck voltage data for all elements are plotted in Figs. 17 and 19. It was felt that graphical presentation of the resistance data, which would consist of decreasing the number of elements, would be both confusing and misleading. Thus the figures include only those elements with resistances below 10.2 mΩ at the end of the test.

The cold junction temperatures increased (ΔT decreased) as the test progressed through the summer months and the temperature of the cooling water increased; toward the end of the test ΔT gradually increased. Similar behavior of ΔT is exhibited by all three groups of elements. It should be noted the apparent relation between decreasing ΔT and Seebeck voltage is largely false. The change in ΔT will account for, at most, a 2.0 mv decrease in the Seebeck voltage. In fact it can be seen that the Seebeck voltage has continued to decrease for all elements, even after ΔT increased at the end of the test.

A number of findings from post-test analysis of these elements are presented in the next section. These findings are highly relevant to the performance of the elements; however, a general discussion of their over-all performance is necessary.
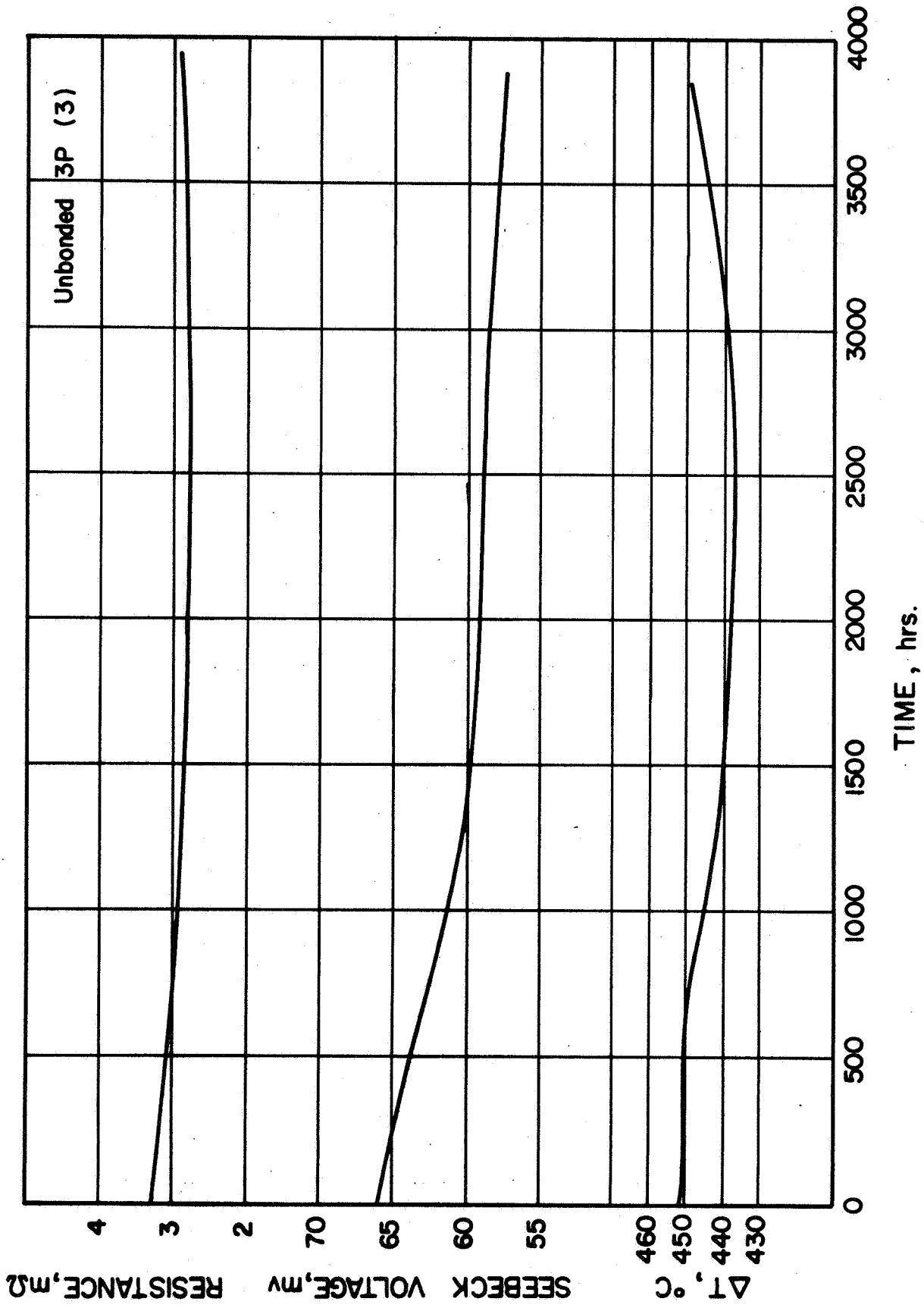
Fig. 17 Life test data on total resistance, Seebeck voltage, and ΔT for three unbonded 3P elements; average $T_H = 510°C$.
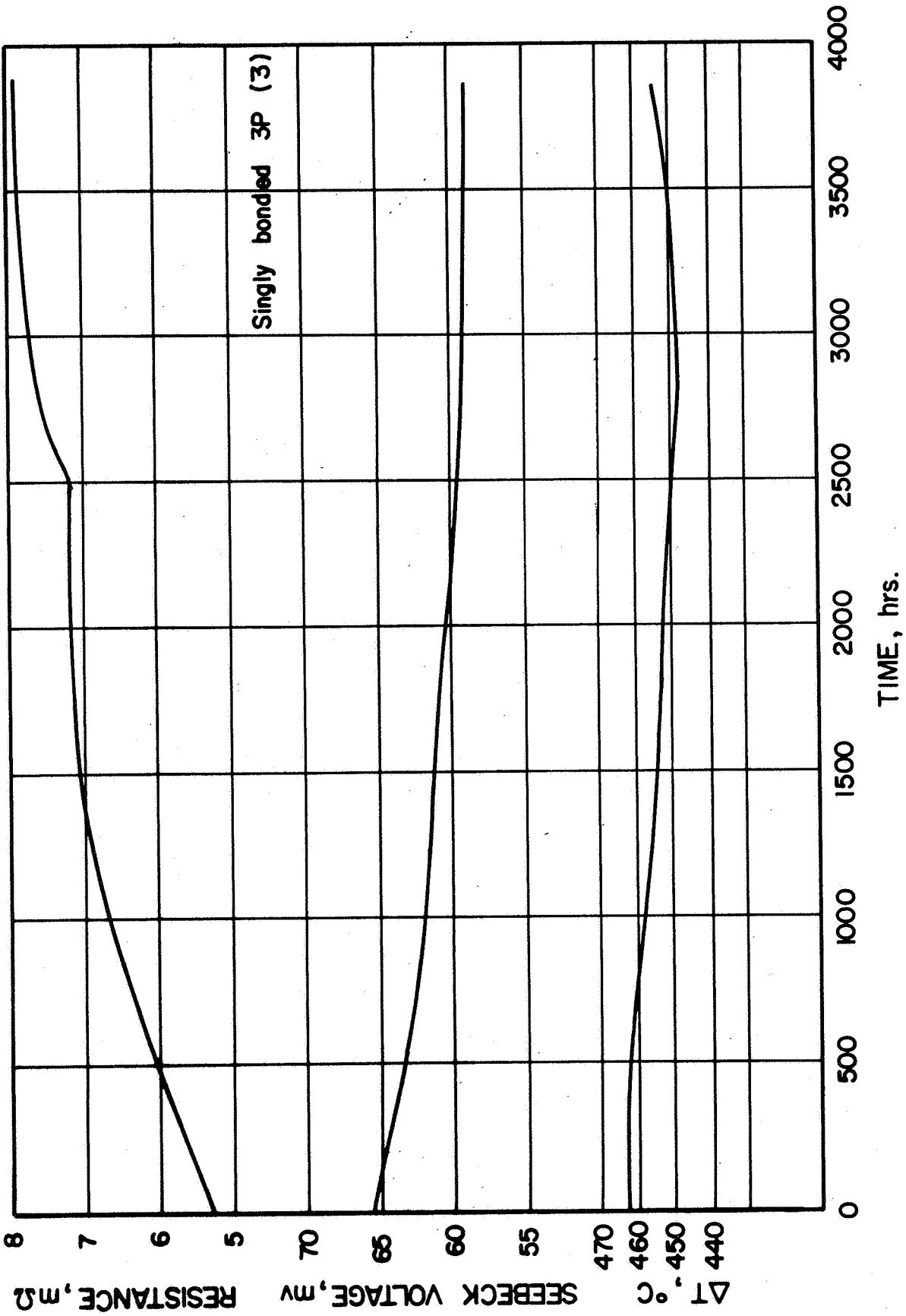
Fig. 18 Life test data on total resistance, Seebeck voltage and ΔT for three W-bonded 3P elements; average $T_H = 510°C$.
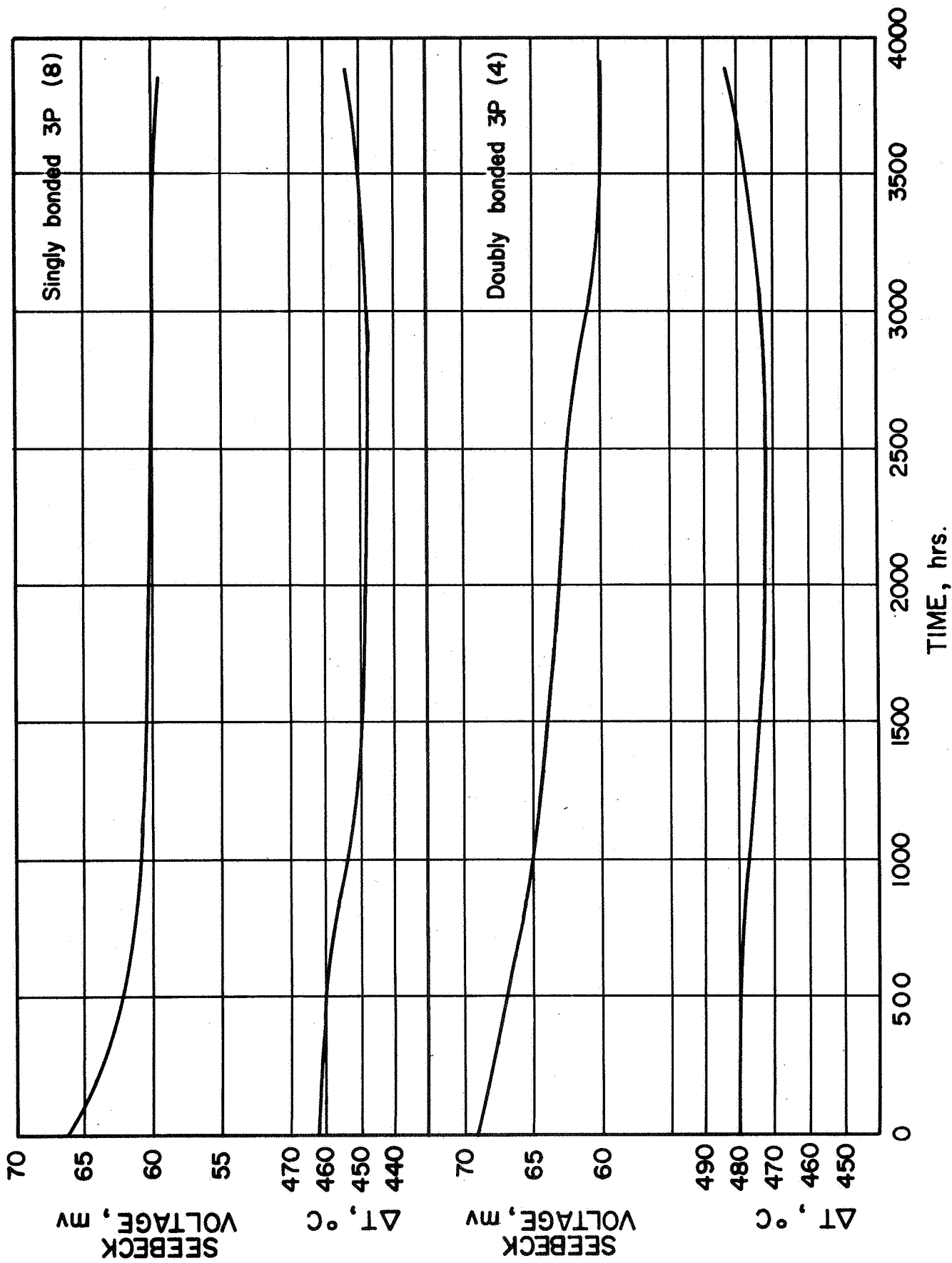
Fig. 19 Life test data on Seebeck voltage and ΔT for single and doubly bonded 3P elements; average $T_H = 510°C$.

The behavior of the W-bonded elements in this test suggest that the major source of increasing resistance is the bond. The Seebeck voltages of bonded and unbonded elements behave similarly. The resistance of the unbonded elements went down, while that of the bonded elements went up substantially. Since it is known that there is no potential for chemical interaction between the electrodes and elements, it must be considered that the bonded elements behave in approximately the same manner as do the unbonded. Seebeck voltage and room temperature resistivity measurements made after the test indicate that this is very likely true.

The assumption that the bonding to W takes place by formation of a substoichiometric lead tungstate (a lead tungsten bronze) may serve as an aid to understanding the behavior of the bonded elements. If oxygen diffuses to the hot contact in sufficient amounts to make up the oxygen deficiency in the lead tungsten bronze, then the junction will become highly resistive, since the stoichiometric lead tungstate, $PbWO_4$, is an insulator. The presence of probably substantial amounts of water vapor and the probable effect on the bonded elements was discussed in the Second Interim Summary Report.

One of the most notable aspects of the behavior of the elements in this test is the steady decrease of the Seebeck voltage. At the end of the test, the voltage of the unbonded elements had decreased 12%, while the bonded elements had decreased 10.5%. This represents approximately a 20% degradation of power, with no change in resistance. In the case of the unbonded elements, the combined decrease in resistance and Seebeck voltage resulted in an equivalent decrease in power, at the end of the test, of approximately 19%.

The bonded elements, of course, showed similar behavior of the Seebeck voltage. The resistance of most of the bonded elements, however, increased as a result of degradation of the bonds. Three bonded elements remained, by comparison, fairly low in resistance throughout the test. Their average resistance, under operating conditions, was approximately 7.9 mΩ at the end of the test compared with 5.2 mΩ

initially. As can be seen in Fig. 18, the resistance of these three
elements had become quite stable by the 2000 hour point. After the
shutdown and restart at 2600 hours, the resistance increased some-
what and then proceeded to level out once more. At the end of the
test, the combined changes in resistance and Seebeck voltage resulted
in an equivalent power decrease of approximately 48%. It was noted in
the Second Interium Summary Report that there was nothing evident
in the initial properties to distinguish these elements from the others.
After the test was terminated, it was noted that these three elements
had substantially smaller deposits of oxides on the contact surfaces
than did the other bonded elements. The pressure on these elements
was slightly less than the average pressure on the other bonded
elements, so that the explanation for their comparative longevity
has still not been found.

At the end of the test, the deflections of the springs maintaining
pressure on the cold sink blocks (and thereby the elements) were
measured, and a load-deflection curve on two springs was determined.
The accuracy of the measurements is uncertain, although good re-
producibility was achieved in determining the load-deflection curve.
If it is assumed that the measurements were fairly accurate, the
range of pressures experienced by the bonded elements was 100 to
195 psi (that is, loads of 5 to 9.5 pounds). No correlation could be
observed between life time and spring pressure. No deformation
of the elements at the hot end was observed, despite the pressure
presumably having been higher during operation due to expansion
of the elements. It is possible, however, that expansion of the cold
junction support rods compensated, or even overcompensated, for
expansion of the elements, thereby reducing the actual pressure
experienced during operation.

Sublimation from the hot portions of the elements appeared
to have been minimal. The test was conducted under approximately
1.1 atmospheres of argon. A very slight rounding of the hot end
corners could be observed in cross section of the elements.

2. Post-Test Analysis of Elements

The Seebeck voltage and room temperature resistivity of the tested elements were measured after conclusion of the test. Several of the elements were also sectioned and the microstructures examined for changes. The results of metallographic measurements to determine whether pore migration had occurred during this test are reported in section IV.

a. Room Temperature Resistivity

The resistivity of the tested elements was measured by a modified four-point probe technique in which one voltage probe moves along the length of the sample while the other is stationary. Four measurements were made on each sample: traverses were made on opposite sides of the sample, starting at the hot end for one pair, and at the cold end for the other pair. Readings were taken every 0.020 inches and plotted as resistance versus distance from the hot end. The resistance values were averaged for the two classes of element; resistivities were then calculated from the average resistance vs. position curves. The resistivity vs. position curves are shown in Fig. 20. It is clear that the resistance of the hot ends of the elements has been substantially decreased. The resistance of the central portions and cold ends of the elements is typical of new or as-bonded elements. The extent of the change in resistivity is approximately equal in both types of element; in fact, the unbonded elements appear to have been affected to a slightly greater distance from the hot junction than the bonded elements. This is an important point to note, for it shows that the decrease in resistivity is very probably not the result of interaction of the element with the hot contact. The bonded elements were, of course, in contact with tungsten, while the unbonded elements were in contact with a more-or-less oxidized Armco iron surface and Chromel-Alumel thermocouple head. Thus, it is most likely that the decreased resistivity is the result of either an internal process due to the gradient or diffusion of an atmospheric impurity into the elements.
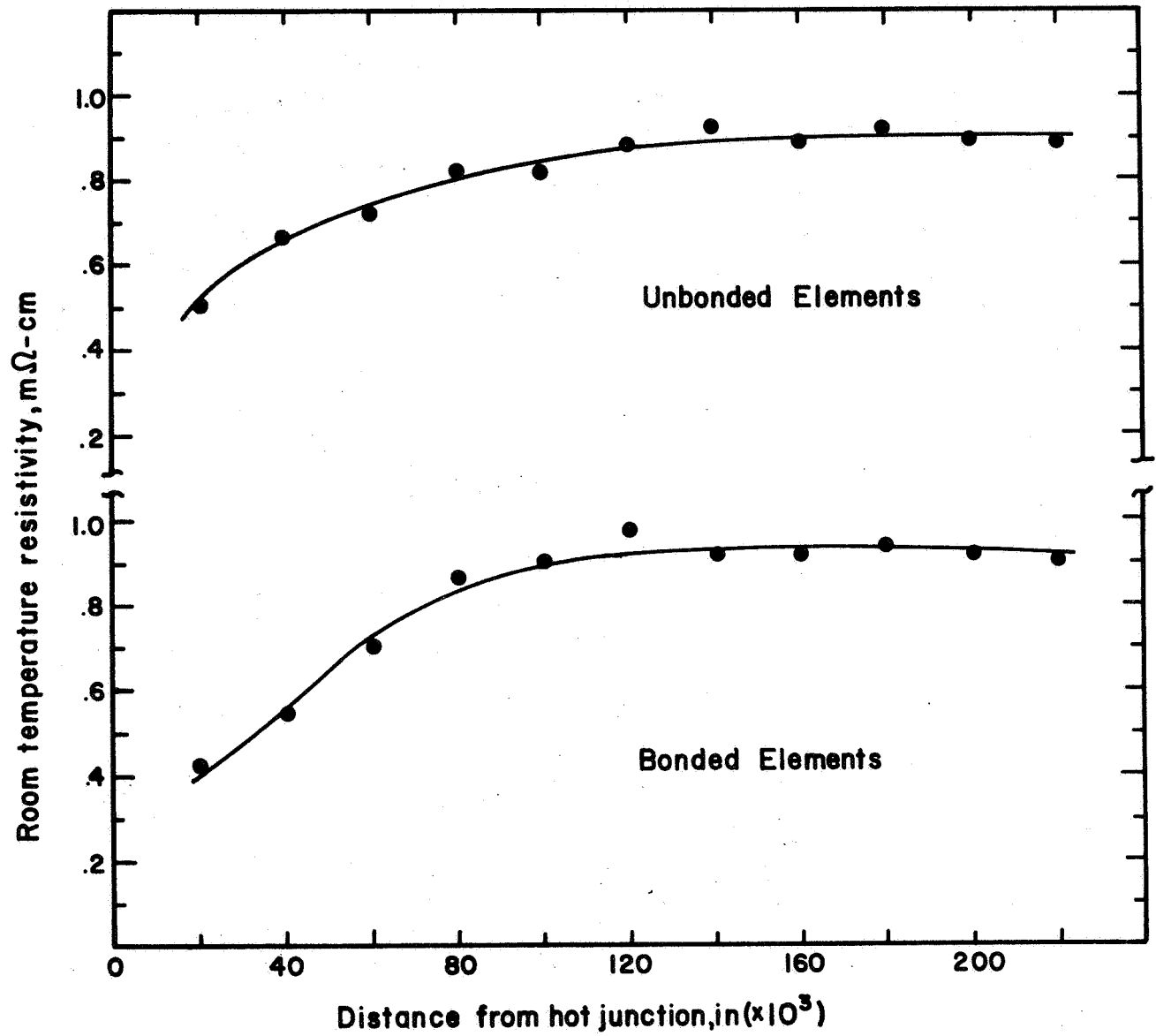
Fig. 20 Variation of room temperature resistivity with distance
from hot end for gradient-tested unbonded and W-bonded
3P elements; average T_H = 510°C for 3850 hours.

A similar effect on the Seebeck coefficient and some possible mechanisms are discussed in sections c and d.

b. Seebeck Voltage

Measurements of the Seebeck voltage of the tested elements were made twice. In one case the hot end during the measurement of the Seebeck voltage was the hot end of the element in the gradient life test; in the other case, the cold end of the gradient test became the hot end in the measurement.

The results of these measurements are listed in Table X. The figures listed are average values from all elements in each category. It is fairly clear from these results that the Seebeck coefficient of the hot portions of these elements has decreased appreciably.

c. Microstructural

Resistivity measurements revealed a number of elements which showed sharp upward discontinuities at approximately mid-element; these were attributed to cracks in the material. Subsequent metallographic examination showed cracks both in the elements which had shown resistance discontinuities and in most of the other elements as well. Figure 21 shows the type of cracks which would appear in the resistivity measurements. In general, the gross cracking tended to run parallel to the longitudinal axis of the element in the cold end and would deviate away at an angle in the middle and hot portion. The course of the cracks was quite irregular and generally determined by the presence of major grain boundaries or areas of precipitation or porosity. All elements showed a certain amount of microcracking. Examples are shown in Fig. 22. Microcracks were generally intergranular, although excursions into the grains would occur with the aid of pores and precipitates.

The origin of the cracks is not obvious from the microstructure; however, it is fairly likely that thermal stress and/or cycling is the cause.
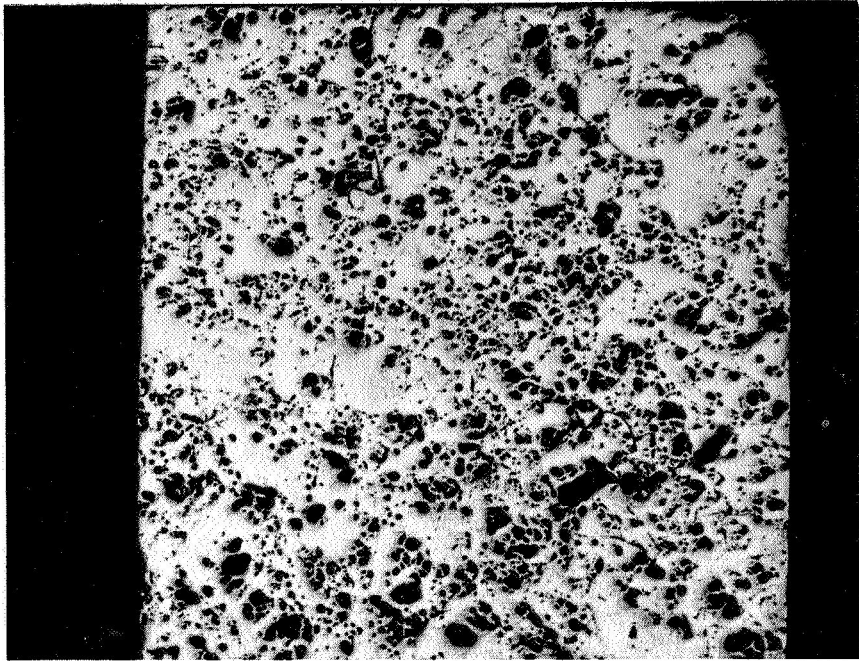
TABLE X

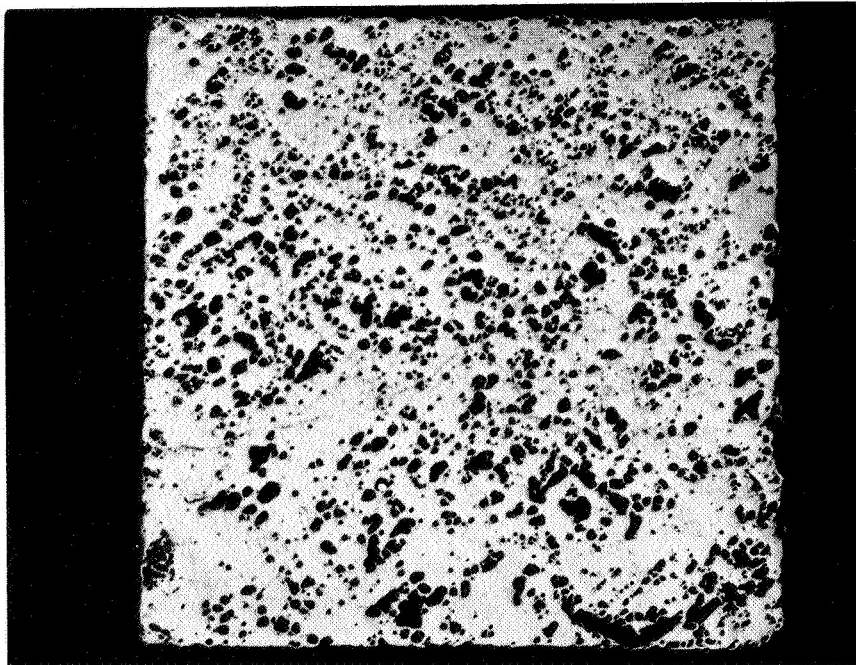### Seebeck Voltage of Gradient Life-Tested Elements

	Pretest S_{500}	Post-test: $S_{500}^{(1)}$	$S_{500}^{(II)}$
	mv	mv	mv
Unbonded (3)	69.5	59	65
Bonded (12)	67	61.5	65.5

(I)   Hot end during life-test is hot end during measurement.

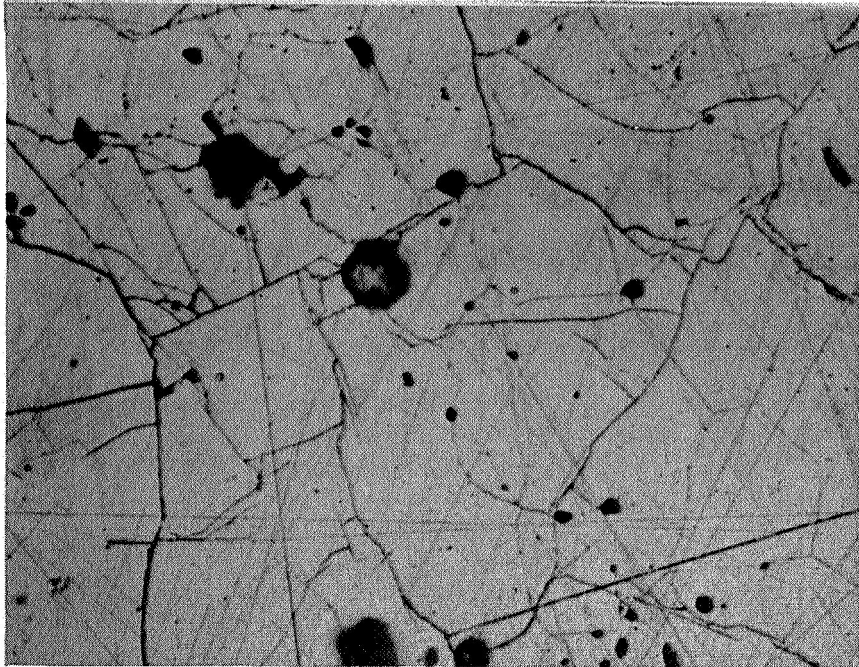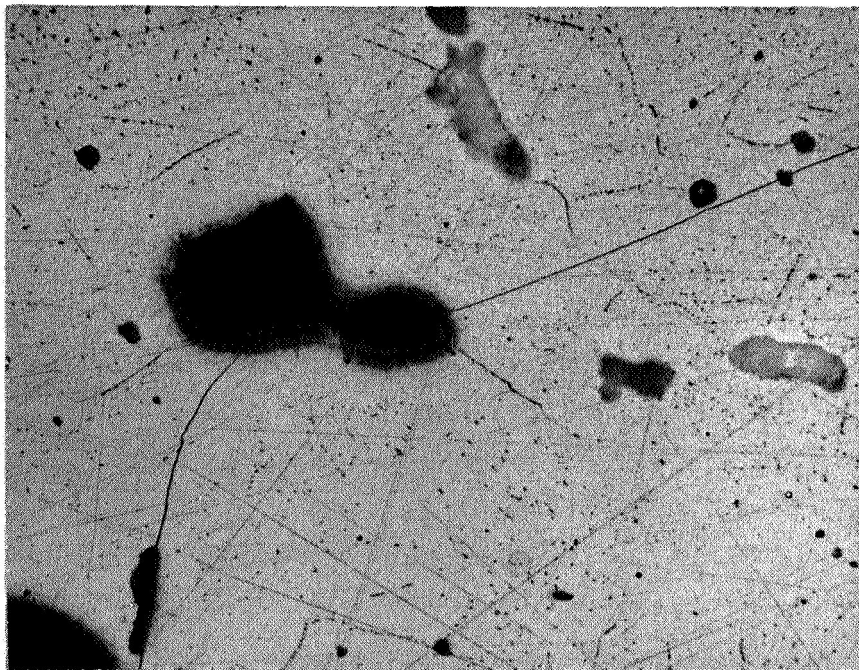(II)   Cold end during life-test is hot end during measurement.

(a)

(b)

Fig. 21   Evidence of gross cracking of gradient-life tested
elements.   14X

(a)

(b)

Fig. 22   Examples of microcracking found generally in
gradient-tested elements.

Elements from the purchase lot designated "P24" showed an unusually large amount of manganese oxide, Fig. 23. Examination of untested elements from the same lot showed similarly frequent occurrence of this phase. Each element showed (on a diametric cross section) five or six clusters of MnO particles of the size of those shown in Fig. 23. Previously, only isolated particles or single clusters of about a dozen particles had been observed (see, for example, p. 95 of the First Interim Summary Report).

Generally, in association with the clustered MnO particles, particles of another phase were found. These can be seen in Fig. 23. It was also found that in all of the elements examined (ten out of fifteen) a band of precipitated particles had formed roughly 0.090 inches away from the hot junction. The transition into this band of precipitation is shown in Fig. 24 (a). The hot side is toward the left of the photomicrograph and the precipitation zone can be best distinguished by the wide grain boundaries. Higher magnification shows that the grain boundaries are sites for precipitation and growth of these second phase particles, as are the interfaces of the matrix and MnO particles (Fig. 23 b). Figure 24 (b) occurred in the bulk of the grains.

The effect was found in bonded and unbonded elements, and elements from three different purchase lots, the first and last of which were separated by a year in purchase date.

An element from the oldest lot showed a lesser tendency toward clustering of the MnO particles, and an apparently smaller amount of MnO. The precipitation zone was further down the element, that is, at a lower temperature, and the morphology of the fine precipitates was less distinct than in the other elements. This is shown in Fig. 25, which also shows clearly, by the depletion of fine precipitates around the central area, that the large particles, nucleated on what is probably a graphite particle, are the same material as the fine, bulk precipitates.
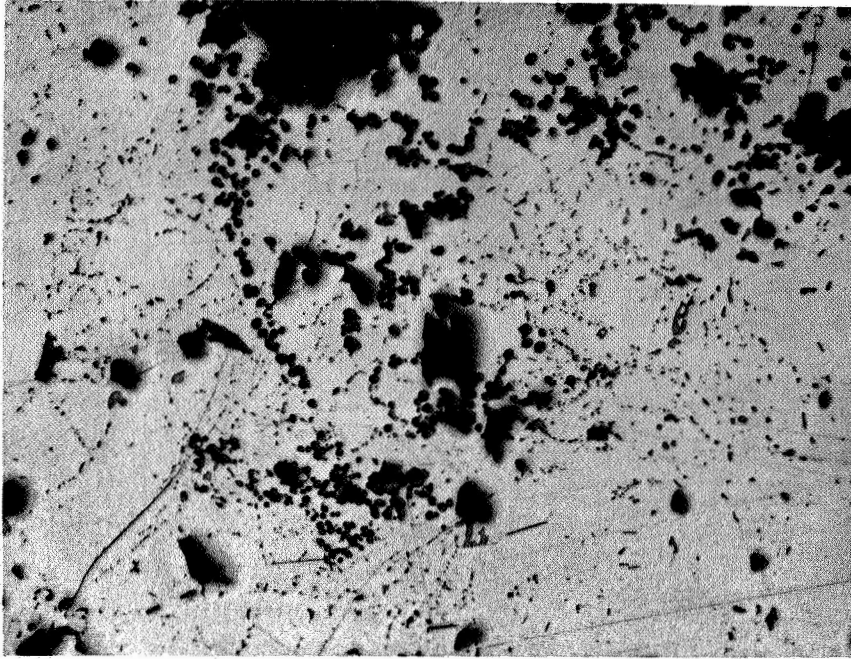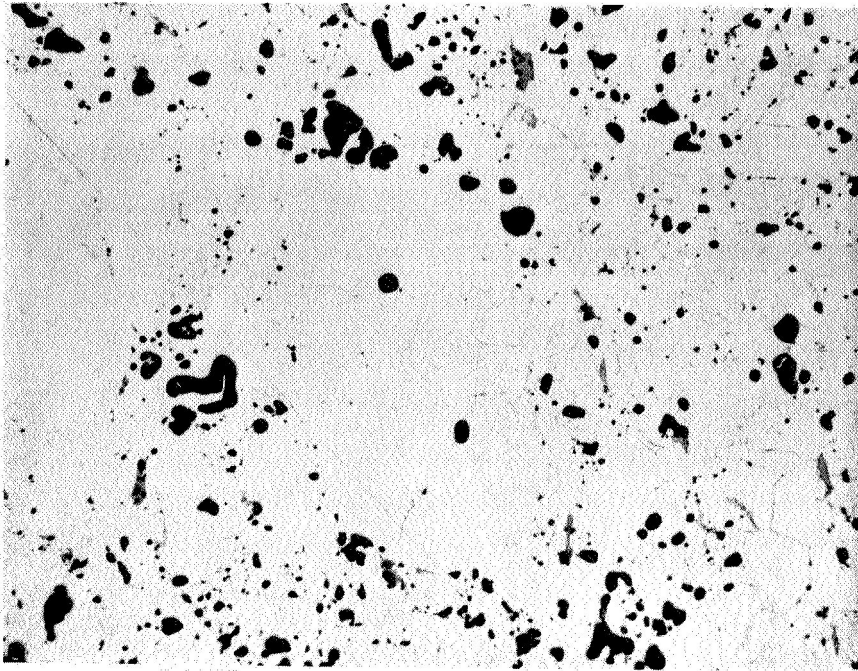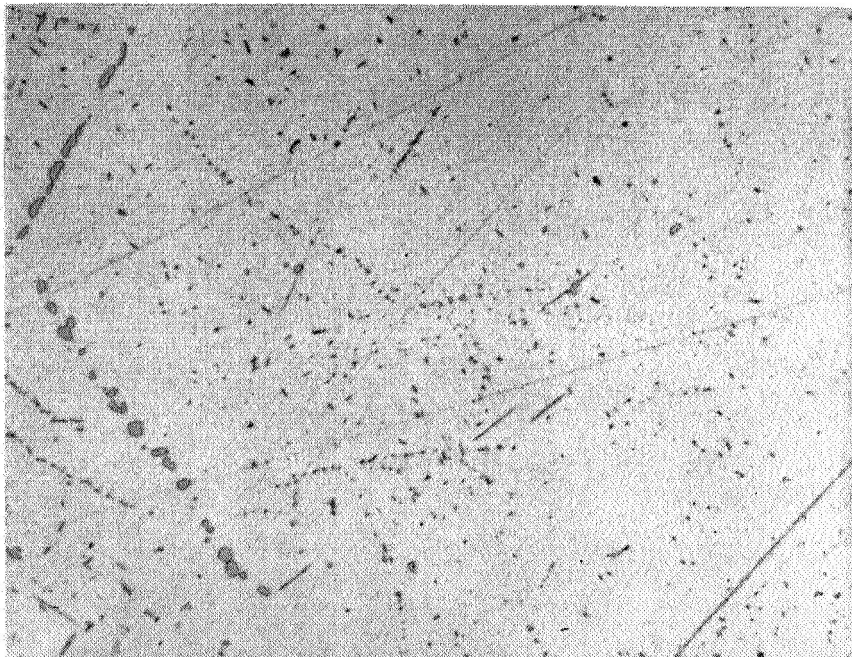
(a)
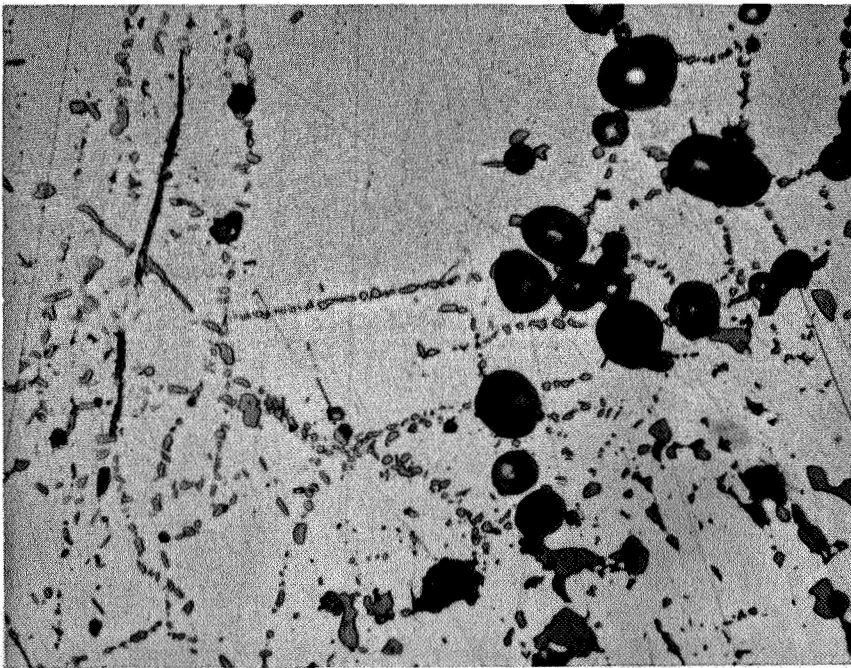
(b)

Fig. 23(a) Manganese oxide particles near hot junction of gradient-
tested 3P element, plus unknown second phase-medium
gray. 150X

23(b) Manganese oxide particles and unknown phase-same
as above. 750X

(a)

(b)

Fig. 24 (a) Transition area into band of precipitation of unknown
             phase in gradient-tested elements. 70 X

        (b) Particles of unknown phase precipitated in gradient
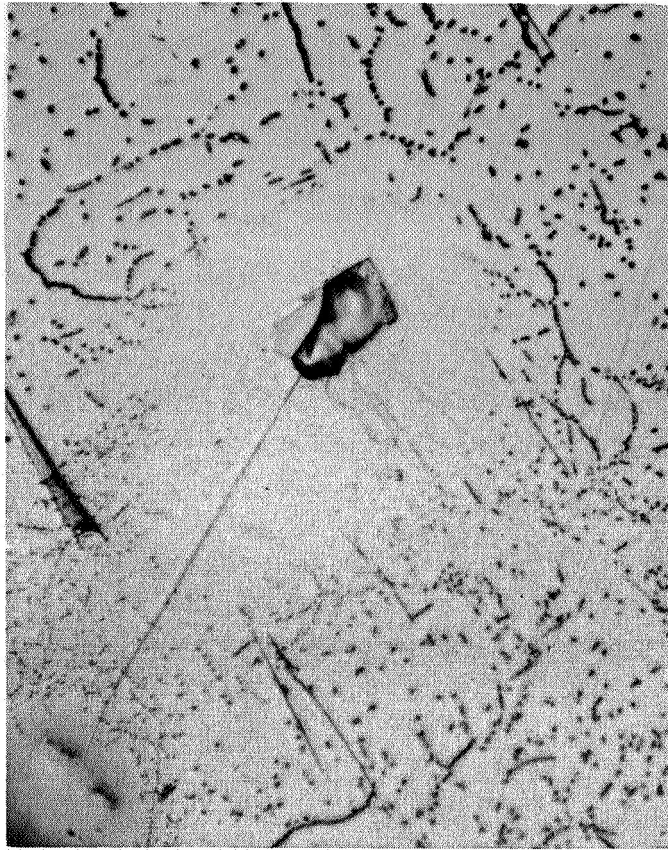   tested 3P elements.   750 X

Fig. 25 Area within unknown precipitate zone showing poorly defined
morphology of particles.   750 X

The general appearance indicates that this phase has pre-
cipitated in the solid state from the PbTe-SnTe matrix. The
existence of what appears to be the same phase at both high (ca. 500°)
and intermediate temperatures (~ 300°) would seem to indicate
that this is more than a simple temperature dependent solubility
effect. However, without positive identification of the phases shown
here, and possibly the development of some of the relevant phase
equilibria, further speculation is not particularly useful.

VI. REFERENCES

1. R. F. Brebrick, Journ, Phys. Chem. Solids 24, 27 (1963).

2. J. I. Umeda, M. Jeong and T. Okada, Jap. Journ. Appl. Phys. 1, (5), 277 (1962).

3. J. W. Wagner and J. C. Woolley, Matls. Res. Bull. 2, (11) 1055 (1967).

4. T. C. Harman, Solid State Research, 3, 5 (1967) Lincoln Laboratory MIT, Report under Contract AF 19(628)-5167.

5. Data for X-ray Analysis, Vol. II, Philips Technical Library W. Parrish, M. G. Ekstein and B. W. Irwin, Editors; North American Philips Co., Inc. Mount Vernon, N.Y.

6. H. E. Bates, F. Wald and M. Weinstein, First Interim Summary Report, Contract #NAS5-9149.

7. H. E. Bates, F. Wald and M. Weinstein, Second Interim Summary Report, Contract #NAS5-9149.

8. H. E. Bates, F. Wald and M. Weinstein, Advanced Energy Conversion 7, 183 (1967).

9. A. G. F. Dingwall, U. S. Patent #3 342567, Sept. 19, 1967.

10. H. Nowotny, F. Benesovsky and C. Brukl, Monatshefte für Chemie, 92, 365 (1961).

11. H. Holleck, F. Benesovsky and H. Nowotny, Monatshefte für Chemie, 96, 570 (1965).

12. P. Stecher, F. Benesovsky and H. Nowotny, Monatshefte für Chemie, 94, 549 (1963).

13. L. H. Brixner, Journ, Inorg. Nucl. Chem., 25, 783 (1963).

14. L. H. Brixner, Journ. Inorg. Nucl. Chem., 25, 257 (1963).

15. F. E. Ashbury and C. Baker, Metals and Materials 1, (10) 323 (1967).

16. S. R. Rocklin, Proc. Intersociety Energy Conversion Engineering Conference, Miami, Florida, 207-219 (1967).

17. H. E. Bates and M. Weinstein, Adv. Energy. Conv. 6, 177-180 (1966).

18. K. H. G. Ashbee, Phil. Mag. 11, 637 (1965).